MACHINE LEARNING MODEL FOR ESTIMATION OF SYSTEM PROPERTIES DURING CYCLING OF COAL-FIRED STEAM GENERATOR

by

Abhishek Navarkar

A Thesis

Submitted to the Faculty of Purdue University

In Partial Fulfillment of the Requirements for the degree of

Master of Science in Mechanical Engineering

School of Mechanical Engineering

West Lafayette, Indiana

May 2020

THE PURDUE UNIVERSITY GRADUATE SCHOOL
STATEMENT OF COMMITTEE APPROVAL

Dr. Jay P. Gore, Co-Chair
School of Mechanical Engineering

Dr. Veeraraghava Raju Hasti, Co-Chair
School of Mechanical Engineering

Dr. Robert P. Lucht
School of Mechanical Engineering

Dr. Li Qiao
School of Aeronautics and Astronautics

Approved by:
Dr. Nicole Key

Dedicated to my family, friends and mentors.

ACKNOWLEDGMENTS

I would like to thank Prof. Jay Gore and Prof. Veeraraghava Raju Hasti for their guidance and support during my academic journey at Purdue University. They helped me at all stages of my research work and kept me focused. I would also like to thank my research team Elihu Deneke, Rathziel Roncancio and Dr. Vikrant Goyal for their constructive feedback. I would also like to thank my committee members, Dr. Robert Lucht and Dr. Li Qiao for their kind feedback. The time I spent at Purdue University was made memorable by all my friends, colleagues and teachers. I would cherish these connections throughout my life.

I would like to acknowledge the Coal Creek Station, Great River Energy, North Dakota, USA for providing the data for this study. Discussions with Craig Miller, Daniel Walsh, and Anantha Narayanan from National Rural Electric Cooperative Association (NRECA); Greg Heinz, David Farnsworth, and Ye Yao from Great River Energy (GRE); Herbert Schaef, Veronica Adetola and Laurentiu Marinovici from Pacific Northwest National Laboratory (PNNL) and Prof. Satish Boregowda from Purdue University are acknowledged and appreciated.

This research was supported by the U.S. Department of Energy under Grant No. DE-FOA-0001989 through National Rural Electric Cooperative Association (NRECA).

TABLE OF CONTENTS

LIST OF TABLES

LIST OF FIGURES

NOMENCLATURE

T: Temperature

P: Pressure

$\dot{W}$: Power

$\dot{m}$ – Rate of mass flow

$\dot{Q}$ – Rate of heat transfer

Subscripts:

SH: Superheater

RH: Reheater

AH: Air heater

$Econ$: Economizer

DSH – Desuperheater

BD – Blowdown

Coal – Pulverized coal

SA – Secondary air

PA – Primary air

FG: Flue gas

FW: Feedwater

In: Component inlet

Out: Component outlet

ABSTRACT

The intermittent nature of renewable energy, variations in energy demand, and fluctuations in oil and gas prices have all contributed to variable demand for power generation from coal-burning power plants. The varying demand leads to load-follow and on/off operations referred to as cycling. Cycling causes transients of properties such as pressure and temperature within various components of the steam generation system. The transients can cause increased damage because of fatigue and creep-fatigue interactions shortening the life of components. The data-driven model based on artificial neural networks (ANN) is developed for the first time to estimate properties of the steam generator components during cycling operations of a power plant. This approach utilizes data from the Coal Creek Station power plant located in North Dakota, USA collected over 10 years with a 1-hour resolution. Cycling characteristics of the plant are identified using a time-series of gross power. The ANN model estimates the component properties, for a given gross power profile and initial conditions, as they vary during cycling operations. As a representative example, the ANN estimates are presented for the superheater outlet pressure, reheater inlet temperature, and flue gas temperature at the air heater inlet. The changes in these variables as a function of the gross power over the time duration are compared with measurements to assess the predictive capability of the model. Mean square errors of 4.49E-04 for superheater outlet pressure, 1.62E-03 for reheater inlet temperature, and 4.14E-04 for flue gas temperature at the air heater inlet were observed.

1. MOTIVATION AND OBJECTIVES

1.1 Motivation

Renewable energy sources are being utilized for electricity generation in the United States with a significantly increased share from 10.6% in 2009 [1] to 19% in 2019. The share is expected to increase further to reach 21% in 2021 [2]. Among the renewable sources, wind and solar constituted approximately 35% of the 19% electricity generation in 2019. The wind energy and solar energy sources are intermittent and contribute to fluctuating demands (i.e., cycling) for power generation from coal power plants. Fluctuating demand for coal also results from the availability of low-cost gaseous fuels and ups and downs in the North American and world economic activities. The resulting cycling operations have impacted many coal power plants severely resulting in significant component damages and financial losses [3]–[6]. As a result, some coal-fired power plants have recently retired [7] and some are on the verge of a shutdown. The remaining coal-burning power plants need to operate safely at optimized costs even under load cycling conditions [4].

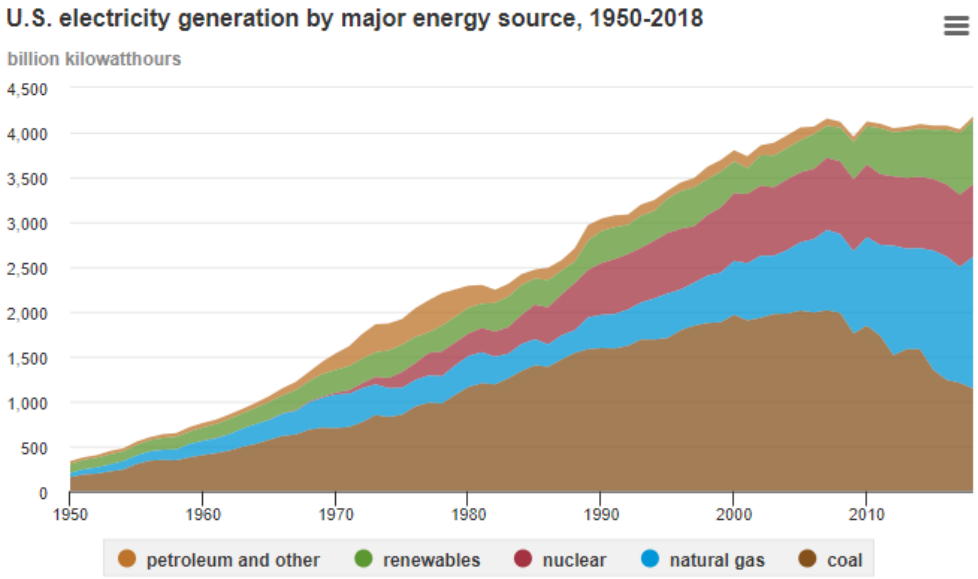

Figure 1.1: U.S. electricity generation by major energy source [1]

The majority (~95%) of the existing coal-fired power plants in the US were designed to operate at baseload conditions with minor load-following [8]. Switching between baseload to

cycling operation affects the maintenance cost and life expectancy of the equipment. The effects of cycling operation are most significant on high temperature and pressure components. The present study considers the steam generation system including air heaters, superheaters, and reheaters. These components experience large temperature and pressure gradients during cycling operations. Schröder et. al. [9] have reported that 52-57% of the cycling-related capital and maintenance costs are associated with the steam generation system.

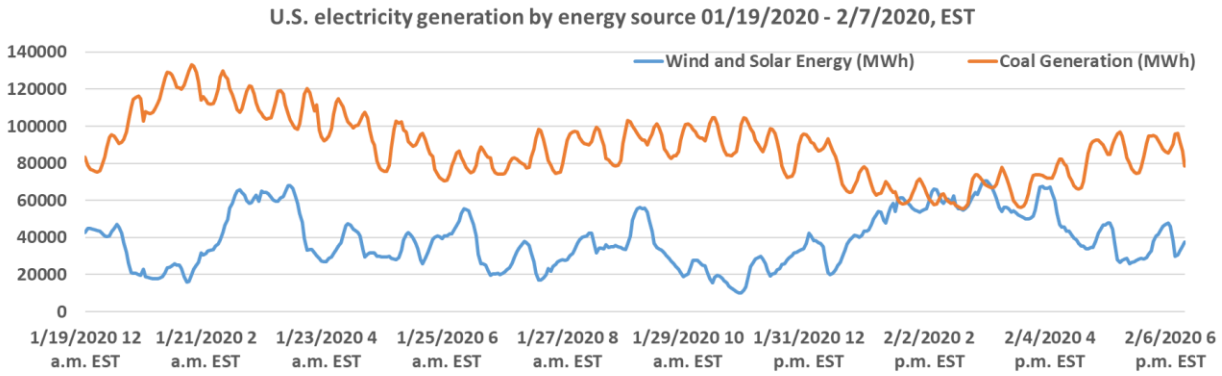

Figure 1.2: Variation of electricity generation with time from coal and renewable sources (wind and solar)

The statistical measures for estimating the cost of cycling power plants considering data from several power plants are reported in the literature [3], [8]–[15]. However, significant variations in the design and operation of power plants exist and unit-specific cost models are more relevant than their statistical counterparts. The life and efficiency of power plant components depend on the variations in the properties during the cycling operation. Hence, it is important to create a model for the estimation of properties to which the components are subjected during cycling operations. Machine learning algorithms are highly effective for relating complex variations of pressures, temperatures, flow rates, and compositions during transient power plant operations. A well trained and validated machine learning model based on the data from an actual power plant can be used to estimate the necessary properties for future cycling operations.

1.2 Objectives

Following are the objectives of the present study:

1. Study the cost associated with cycling operation
2. Identify cycling operations from the gross power data of a coal powerplant
3. Develop a relationship between power plant load cycling and variation of system properties using Artificial Neural Networks (ANN)

2. LITERATURE REVIEW

2.1 What is Cycling?

The operation of electricity generation units at varying load levels in response to varying dispatch requirements is called cycling [10]. This includes on/off operation and load-follow cycling operation. As opposed to cycling, baseload operation corresponds to the continuous operation of a power plant at the designed nominal capacity. Cycling is caused by the change in the demand. Since electricity is not stored, its production must always match the demand. The demand for electricity varies with time of the day, day of week, and seasons. Such variations in demand were predictable and the need for cycling power plants was relatively low. However, as the integration of variable renewable energy sources is increasing the fluctuations in the electricity demand have increased forcing increased cycling of conventional power plants.

Le et. al. [16] presented the pros and cons of cycling units from the perspective of a system operator and plant personnel. The flexibility afforded by cycling is an asset for the system operator. A system operator tries to minimize the total generation costs by considering factors such as minimum loads, changing load forecasts, forced outages, and opportunistic purchase and sale transactions. The authors reported a 1.5% reduction in operating cost when the minimum up/down time requirements for units was reduced from 168 hours to 12 hours. The flexibility of cycling units with short start-up times is advantageous as the unit commitment software can then react to the changing load forecasts.

On the other hand, plant personnel try to maximize the unit efficiency and minimize equipment stress. The electricity generation units were designed and optimized to operate at the maximum capacity and hence the efficiency of the power plants changes when operated at a reduced capacity. Also, these units were designed for continuous operation rather than a cycling operation. Cycling causes the heat-rate to increase and shorten the equipment lifetime. As compared to controlled shutdowns which are relatively risk-free, forced shutdowns can lead to higher equipment damage due to sudden interruptions and large temperature gradients. These hidden costs make cycling undesirable for plant operators. The impact of cycling operations can be categorized as load efficiency cost, capital and maintenance cost, and forced outage cost.

Several studies have tried to include the cycling cost in the unit commitment models [17]–[19]. Bergh et. al. [17] studied the impact of cycling parameters of conventional generation units to determine the optimal scheduling of the electricity generation system by simulating. The cycling of conventional units is simulated using a commitment model, demand time-series, renewable generation time-series and a model for the electricity grid. Four weeks of data at 15-minutes resolution was used. All types of cost of cycling: direct start costs, indirect start costs, forced costs, ramping costs and efficiency costs were considered. These costs were estimated using data provided by [9] and [10] which was based on statistical studies of various power-plants. Bergh et. al. concluded that the cycling cost can be reduced by 40% by considering all cycling costs in the unit commitment scheduling.

Corio et. al. [8] noted in an EPRI report that the metrics used to define cycling vary between different studies. Engineering firms that design and build power plants classify cycling as on/off cycling, also known as two-shifting, and load cycling. The electric industry sources, like the North American Electric Reliability Council (NERC), classify the power plant operation in 5 categories: (i) Baseload with minor load following, (ii) Periodic startup, load follow daily, reduced load nightly, (iii) Weekly startup, load follow daily, reduced load nightly, (iii) Daily startup, load follow daily, off-line nightly and (v) Startup chiefly to meet daily demand. Previous statistical studies [10] have looked at the number of different types of start-up operations, the number of load-follow operations and their ramp rates as metrics for the estimation of cost of cycling. Corio et. al proposed 14 functional forms for defining the metrics of cycling operations. These functional forms were close to the categories used by NERC and had attributes such as frequency, periodicity, and amplitude.

2.2 Capital and Maintenance (C&M) Cost

When the power plant is operated it causes damage to the generating units. The operation can be under base-load or cycling conditions. The damage accumulated by the power plant is due to a combination of mechanisms such as creep, fatigue, erosion and corrosion [14], [20]–[22]. Creep damage occurs when components under stress are subjected to high temperatures. Under base-load conditions, the system properties such as pressures and temperatures remain relatively constant leading to creep conditions. Powerplants are designed to operate under these conditions using creep-resistant materials. The variation of temperatures and pressures experienced by

components during cycling conditions causes damage due to fatigue. During cycling operations, both creep and fatigue mechanisms are active for high-temperature components leading to premature failures. This is known as creep-fatigue interaction.

Shibli et. al. [21] provides a brief overview of component failures resulting from creep-fatigue interaction. Thick wall components such as the boiler are prone to thermal fatigue cracking. Superheater and reheater header ligament can experience thermal fatigue cracking due to poor temperature control. The expansion and contraction of the furnace wall tubes during cycling operation is not uniform and causes internal stress which can eventually lead to thermal fatigue cracking in the evaporator and economizer headers. The pipes in the boiler are attached to the furnace walls or other pipes using slip ties and brackets. Failure of these attachments due to thermal variation is one of the main causes of forced shutdowns.

Component level studies have been reported for estimation of the remaining life of components [20]. Creep-fatigue interaction was identified as the key damage mechanism. Creep damage depends on the dwell time for which the component is exposed to high temperatures while fatigue damage depends on the number of cycling operations. The cumulative damage due to creep and fatigue can be estimated using four main techniques: linear damage summation analysis, frequency-modified strain range analysis, strain range partitioning analysis and ductility exhaustion analysis. All these techniques depend on data coming from laboratory testing of materials used in the components. This affects the accuracy of the component life estimation as uncertainties in plant operation are not accounted for.

Statistical models for the estimation of cost of cycling involves a collection of plant or unit-level data from several plants. These studies also lack inaccuracy as it is extremely difficult to distinguish the cost associated with wear and tear due to normal operation from that due to cycling operation. For a typical large (300-900MW) coal-fired sub-critical steam power plant, the average C&M cost for load-following cycling operation was estimated to be 2.45$/(MW capacity) by Lefton et. al. [10]. This cost was reported in terms of the 2011$ amount. The cost was multiplied by a factor ranging from 1.5 to 10 for higher ramp rates. Corio et. al. [8] proposed a methodology for estimation of the cost of cycling using the functional form for defining cycling operations.

2.3 Forced Outage Cost

The rate of damage accumulation increases due to cycling operations which leads to an increased number of forced outages. The reliability of the power plant can be measured in terms of Equivalent Forced Outage Rate (EFOR) which is a ratio of offline hours during demand to the total number of service hours. If the power plant must procure replacement power, the cost of increased EFOR includes the lost revenue and the cost of replacement power. The effect of cycling operations on EFOR has been reported in [10]. The study was conducted for 10 similar steam-electric units. An increase in the number of cycling operations is followed by an increased EFOR. However, the increase in EFOR is not immediate. As the plant gets older, it starts to accumulate more damage due to cycling leading to more frequent forced outages.

After a forced outage, additional resources are required to bring the boiler back online. The startup cost includes the cost of materials such as fuel, water and chemicals. The cost associated with auxiliary power must also be included if supplied during startup. Increased manpower is required during startup as compared to base-load operation. This is reflected in the increased labor costs. During ramp-up or ramp-down operation, the boiler efficiency is also lower than the base-load operation. The cost of replacement power to be purchased during the offline hours is a major part of the cost associated with forced outages.

Ramping-up the output of a unit after shutdown also leads to significant damage to components leading to higher maintenance and capital expenditures as described in section 2.2. The damage to the components depends on the range and the rate of change of the temperatures and pressures [8]. Hence, the startup costs vary significantly with the type of startup classified based on the downtime of the unit. A warm start refers to startup operation after 12-40 offline hours. If the number of offline hours is lesser than 12, then it's referred to as a hot start. Cold start corresponds to startup operation after 40 of offline hours. During a cold start, the power plant components experience a larger range of temperature as compared to a hot start. These classifications are based on [10] for large sub-critical coal-fired power plants.

The capital and maintenance cost associated with startup operations is challenging to estimate. Keatley et. al. [23] created a statistical model for forecasting the cost of a hot, warm or cold start as a function of the unit's service life. They considered 19 power-generation units from the Irish Single Electricity Market (SEM). Out of these 19 units, 5 were coal-fired conventional units, 4 were gas-fired conventional units and 10 were combined-cycle gas turbine (CCGT) units. The

operation and cycling cost data in the European Technology Development (ETD) database was used to estimate the annual non-fuel operation and maintenance (O&M) cost for the units in the Irish system. This cost was related to the unit's actual consumption of service life. Per-start cost for the unit was calculated by dividing the annual O&M cost by the number of starts per year. The cost due to the long-term increase in heat rate, increased forced outages and foregone energy payments was not included. The resulting cost data for the units was studied with the creep life and fatigue life. The creep life was determined in terms of on-line hours and the fatigue life was determined based on the number of startup operations. Correlations relating the annual O&M cost to creep life and fatigue were derived. They noted that the creep life does not strongly relate to the O&M costs whereas there is a strong correlation between the fatigue life and the O&M costs.

Kumar et. al. [10] have provides a good overview of power plant cycling costs and systems commonly affected by cycling. They analyzed detailed cost data for several hundred units in North America. These units included various coal-fired and gas-fired power plants. Table 2.1 shows the lower bound cycling costs for a typical large (300-900MW) coal-fired sub-critical steam power plant [10]. All costs are in 2011$ amount.

Table 2.1: Cost of cycling for large coal-fired power plants [10]

Operation	**Cost item**	**Median value**
Hot start	C&M ($/MW capacity)	59
	EFOR (%)	0.0057
	Startup fuel (MMBTU/MW capacity)	7.50
	Other startup costs ($/MW) (aux power, chemicals, water, additives, etc.)	5.61
Warm start	C&M ($/MW capacity)	65
	EFOR (%)	0.0070
	Other startup costs ($/MW) (aux power, chemicals, water, additives, etc.)	7.98
	Startup fuel (MMBTU/MW capacity)	10.00
Cold start	C&M ($/MW capacity)	105
	EFOR (%)	0.0088
	Startup fuel (MMBTU/MW capacity)	14.00
	Other startup costs ($/MW) (aux power, chemicals, water, additives, etc.)	10.15

2.4 Efficiency Cost

Since most of the coal-fired powerplants were not designed for cycling operation, their efficiency is generally lower when operated at below maximum capacity [10], [14]. This includes the ramp-up and ramp-down during startup and shutdown. The heat rate, which is a ratio of the energy input to the system and electricity generated, increases as the power plant is operated at lower output [12]. As the power plant accumulates damage, the heat rate further increases. One study has estimated this increase to be about 0.44% per startup operation for large subcritical coal-fired power plant [10].

2.5 Machine Learning in Power Plants

In [10] Kumar et. al. noted that "use of the cycling cost numbers without accounting for actual unit operations can result in significant under/over estimation of power plant cycling costs." All the categories of the cost of cycling discussed in the previous sections depend on the variation of the system properties during cycling operation. Hence, to accurately estimate the cost of cycling, it is important to create models that can estimate this variation of the system properties. A power plant is a highly complex system of systems. The physical laws that govern these systems involve parameters such as friction coefficient of pipes, heat transfer coefficients, etc. that are specific to the power plant under consideration. Also, the values of these parameters change over time. An example of such a change was discussed in section 2.3 where it was noted that the plant accumulates damage at a faster rate as it grows older. Hence, estimating the variation of system properties during cycling operation is challenging using only the physical equations. Machine Learning models are very useful for such problems. Using the power plant operation data, very complex relations can be derived between the input and output variables. Once trained, these models can estimate system properties for cycling operation quickly as compared to detailed power plant simulations.

Studies have been conducted using measurements [24]–[31] as well as results of simulations [32]–[36] from power plants as inputs to machine learning algorithms for boiler models. Kljajić et. al. [37] implemented an ANN model for predicting the boiler efficiency. The data for this model was collected by surveying 65 boilers from various sectors such as industrial, district heating systems, and healthcare facilities in Serbia. The input variables for the ANN model were the type

of fuel, type of boiler, oxygen content in flue gases, exploitation period, normal capacity, and load range. Liu et. al. [27] compared the linear model, neural network, and fuzzy neural network for prediction of power output, steam pressure, and separator outlet steam temperature using real data from an ultra super-critical steam boiler.

Smrekar et. al. [24] examined the feasibility of developing an Artificial Neural Network (ANN) model for a boiler of a coal-fired power plant. The objective of the model was to predict the mass flow rate, temperature, and pressure of the steam exiting the boiler using the mass flowrate of coal, opening of the boiler valve, and the feedwater pressure. The input variables were chosen after performing a sensitivity analysis by evaluating the ANN model with different sets of input variables. The set of input variables for which the ANN model had the least error was chosen. The coal mass flowrate used for training the ANN model was calculated using the known boiler efficiency and calorific value of coal. An alternate ANN model was created by replacing the calculated mass flow rate of coal as input by the conveyor speed. The model was trained and validated using 12 days of real coal-fired power plant in Slovenia with a 1-minute resolution. Sections of data corresponding to rapid changes and off-nominal load operation were excluded from the training set. In [25], Smrekar et. al. used a similar method to train ANN models for boiler and turbine using one month of data for a power plant in India with a 30-minute resolution. They integrated these two models for predicting the power output of the plant. This study was also based on only steady-state data.

Very few studies have incorporated the transient data in the machine learning models for boilers [26], [28], [30]–[32]. Smrekar et. al. [26] compared linear and non-linear models for multi-step-ahead prediction of NOx. The linear models included an auto-regressive model with exogenous inputs (ARX) and auto-regressive moving-average model with exogenous inputs (ARMAX) models while the non-linear models included artificial neural networks and support vector regression models. These models were trained and validated using 9 days of data including transient operations. The original data with 10-second resolution was resampled to obtain a resolution of 1 minute. The inputs for these models were selected from a set of 32 variables such as conveyor belt speed, air flowrates, steam pressure, steam flow rate, air-fuel ration, etc. after conducting a sensitivity analysis. The ARX model was found to have the least mean absolute error.

Oko et. al. [32] adopted the nonlinear auto-regressive with exogenous inputs (NARX) neural network for predicting the boiler drum pressure and water level. NARX is a type of recurrent

neural network (RNN) that predicts an output variable based on the time history of the output variable and the current value and the time history of input variables. The inputs to the NARX model used in this study are the heat input, steam flowrate, and feedwater flowrate. A synthetic dataset was created by simulating a 160 MWe coal-fired power plant. The inputs were perturbed with a series of step changes to incorporate randomness in this synthetic dataset. The final dataset had a duration of 3 hours with a 1-second resolution.

Laubscher et. al. [28] developed a model for forecasting the reheater metal temperature in a coal-fired power plant. An encoder-decoder Gated Recurrent Unit (GRU) framework was used with an input sequence of length 8 and an output sequence of length 5. The time-series data had a resolution of 1 minute. The input sequence represents the 8-minute history of 92 parameters such as wind-box pressures, fuel flow rate, boiler load, primary fan parameters, induced fan parameters, ambient conditions, reheater metal temperatures, etc. The output sequence represents the 5-minute prediction of the reheater metal temperatures. The data for training the model was collected from a 290 MWe drum-type boiler for 10 days with a 1-minute resolution. An extensive hyperparameter search was performed to find the optimal model. Root-mean-squared error (RMSE) of 6.2 ^{0}C was observed on the test set.

3. EXPLORATORY DATA ANALYSIS

3.1 Coal Creek Station

The data used in this study was collected from the Coal Creek Station (CCS) owned by the Great River Energy. It is an 1100 MW lignite-based power plant in North Dakota. It has two tangentially fired Combustion Engineering Circulation boiler units each rated at 550 MW. A schematic of the steam generator is shown in Figure 3.2. The boiler was designed for 1005 F main steam and reheat steam temperature at a pressure of 2520 psig for feedwater temperature of 490 F. The boilers use lignite with a typical higher heating value of 6800 Btu/lb and moisture content of about 36.6%. The superheater steam temperature is controlled by interstage desuperheating and reheater steam temperature is controlled by fuel nozzle tilt. Reheat desuperheaters are also provided in the cold reheat piping in case of an emergency.

Figure 3.1: Aerial photo of the Coal Creek Station

There are eight pulverizers connected to the windbox by 20-inch pipes. The ignition energy is provided by four oil guns and high energy arc ignitors. The steam generator has two air preheaters, two primary air fans and two forced draft fans. The air preheaters are designed to heat the output of the primary air fans for delivering primary air at 768 F to the pulverizers. The cold primary air (output of the primary air fans) can be mixed with the hot primary air via tempering

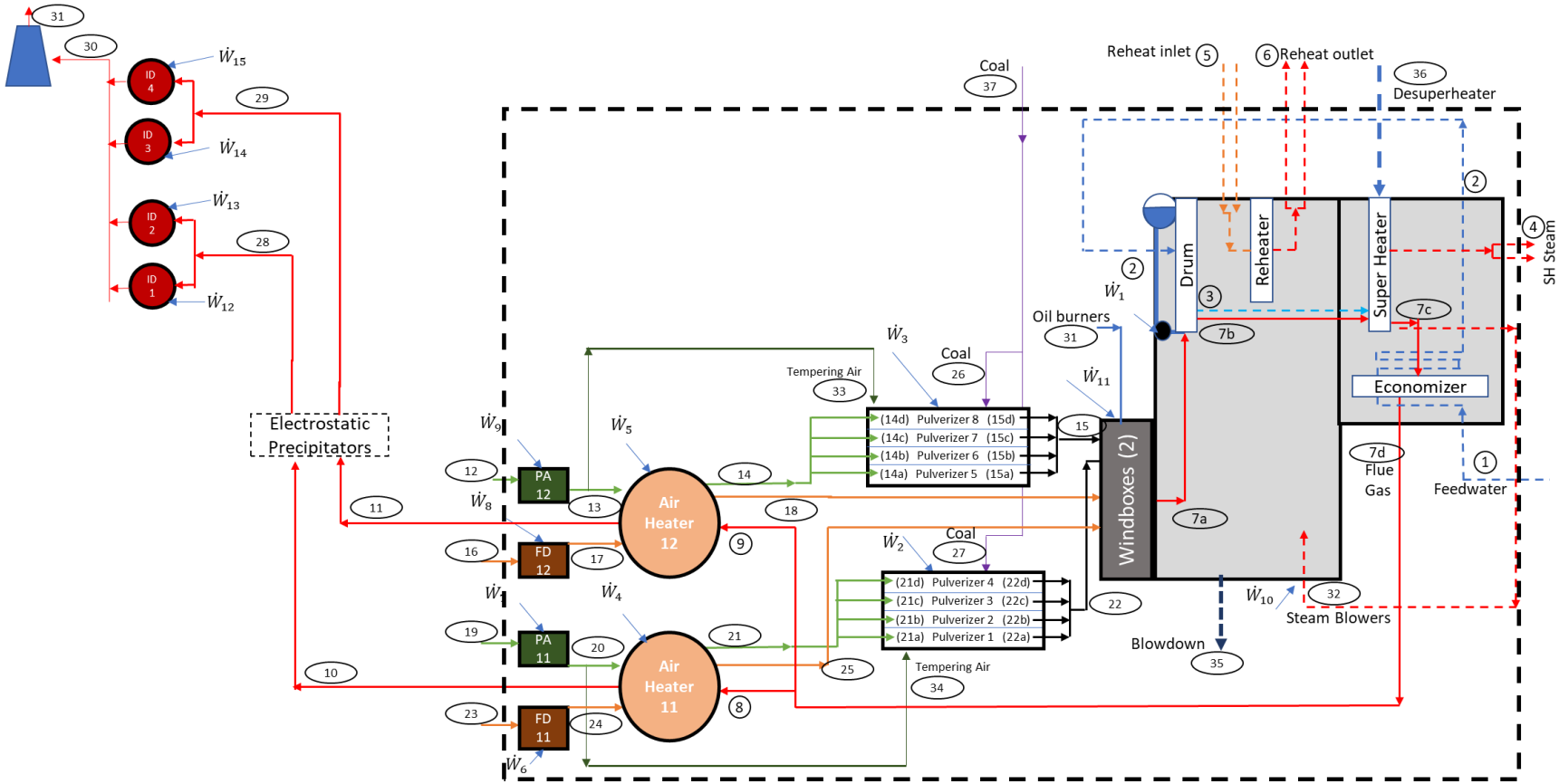

Figure 3.2: Schematic diagram of the steam generator with components

dampers for maintaining the temperature required for fuel drying in the pulverizers. The air preheaters supply secondary air at 741 F to the windbox using the output of the forced draft fans. The flue gas entering the air preheaters is cooled from 838 F to 338 F. The furnace has 28 soot blowers and 170 wall blowers. A schematic of the steam generator is shown in Figure 3.2.

3.2 Outlier detection

Data from the Coal Creek Station was available as 1-hour averaged time-series from 2010 to 2019. The data collected from the power plant contains outliers and needs to be cleaned. There are three types of outliers [38]:

1. Global outliers
2. Contextual outliers
3. Collective outlier

Global outliers correspond to data points that are significantly different from the rest of the data. For example, the time-series of gross power contains unphysically high values like 60000MW. Such outliers are removed by defining the range of value that a property or variable can physically exhibit. In the case of gross power, the range is set to 0 to 650MW. Figure 3.3 shows the variation of gross power with time after the removal of global outliers. The range of values set for global outlier detection is given in Table 3.1.

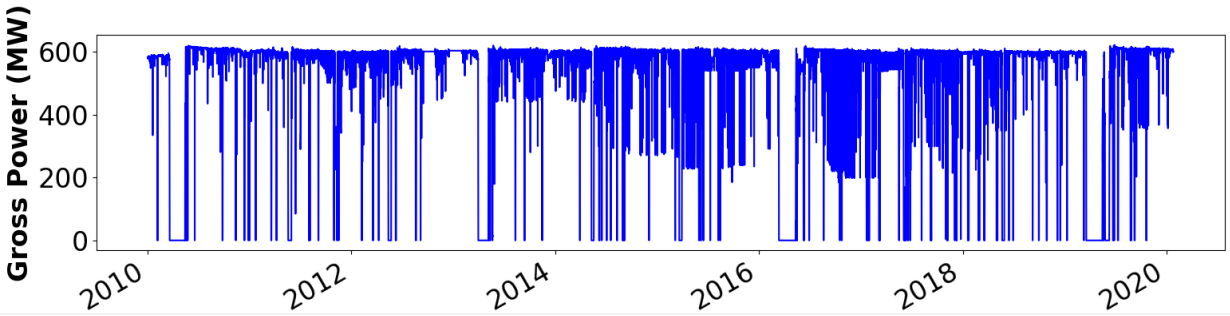

Figure 3.3: Variation of gross power after removing outliers

Table 3.1: Range of properties for global outlier detection

Property/ Variable	State (Figure 3.2)	Tag	Min value	Max value	Units
$\dot{m}_{FG,AH\_Out}$	10	AHT_11_GASOUT:Flow	0	4000	klb/hr
T_{FG,AH_Out}	10	AHT_11_GASOUT:Temperature	0	400	F
$\dot{m}_{BD}$	35	BLOWDOWN_SIG:Flow	0	150	lb/hr
$\dot{m}_{FW}$	1	FEEDWATER:Flow	0	4500	klb/hr
P_{FW}	1	FEEDWATER:Pressure	0	3500	psia
T_{FW}	1	FEEDWATER:Temperature	0	300	F
P_{SH_Out}	4a	MAIN_STEAM:Pressure	0	3500	psia
T_{SH_Out}	4a	Plant_Measurement:DCS_SGT406U2	0	1050	F
P_{RH_In}	5a	COLD_REHEAT:Pressure	0	700	psia
T_{RH_In}	5a	COLD_REHEAT:Temperature	0	650	F
P_{RH_Out}	6a	Plant_Measurement:DCS_2SG256AI	0	650	psia
T_{RH_Out}	6a	Plant_Measurement:DCS_SGT413U2	0	1050	F
$\dot{m}_{PA,AH\_In}$	19	AHT_12_PRI_AIRIN:Flow	0	4000	klb/hr
P_{PA,AH_In}	19	FAN_PA_22:Total_Static_Press	0	45	In Wg
T_{PA,AH_In}	19	FAN_PA_22:Inlet_Temp	-30	120	F
$\dot{m}_{SA,AH\_In}$	16	FAN_FD_21:Mass_Flow	0	2500	klb/hr
P_{SA,AH_in}	16	FAN_FD_21:Total_Static_Press	0	15	In Wg
T_{SA,AH_in}	16	FAN_FD_21:Inlet_Temp	-30	120	F
$\dot{W}_{gross}$	-	GEN:Power	0	650	MW
$\eta_{SG,IO}$	-	SG_IO:Efficiency	0	100	
$\dot{Q}_{SGI}$	-	SG_IO:Heat_input	0	7500	MBtu/hr
$\dot{Q}_{mainSteam,SGO}$	-	SG_IO:Heat_reheat	0	1200	MBtu/hr
$\dot{Q}_{reheatSteam,SGO}$	-	SG_IO:Heat_mainsteam	0	4500	MBtu/hr

Conditional outliers correspond to data points whose values may not be perceived as anomalous, but the data point is an outlier for a given condition. These outliers are within the range defined in Table 3.1 but are unphysical. For example, in Figure 3.4, the superheater outlet steam pressure (main steam pressure) and the superheater inlet steam pressure is 0 even when the gross power is not equal to 0 and vice versa during multiple instances. Data points corresponding to such conditions are removed from the dataset.

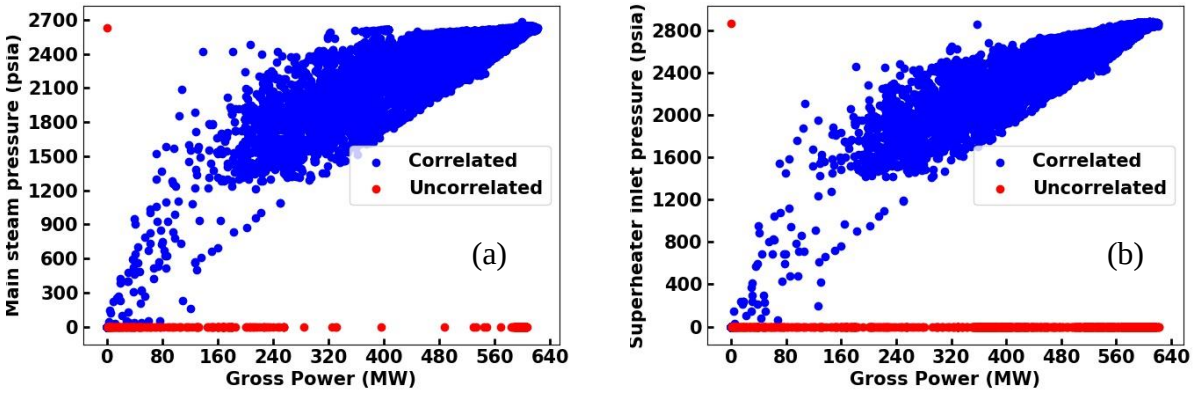

Figure 3.4: (a) Superheater outlet pressures (main steam pressure) and (b) superheater inlet pressure vs. gross power

Collective outliers correspond to data points which are outliers as a group but not individually. For example, if the value of a superheater outlet pressure remains constant to the last significant figure over a long duration, it indicates a sensor failure or problem with data retrieval. Such outliers are difficult to find in the time-averaged data and are not filtered out in the present study.

3.3 Identification of cycling operations

It was noted in section 2.5 that the cost of cycling power plants depends on the operation history of the unit. Hence, it is important to identify the cycling operations from the operation history of the power plant. A typical cycling operation is illustrated in Figure 3.5 and consists of a constant power operation between 10 and 14 hours on 8/27/2019 followed by a ramp-down segment with three rates between 14 hours and 16 hours, followed by a constant power operation between 16 and 18 hours followed by a ramp-up segment between 21.5 hours, finally terminating in a constant segment between 21. 5 hours and 24.00 hours. The ramp-up and ramp-down segments have smaller sub-segments of different ramp-rates. The cycling operations are identified by finding instances corresponding to the starting point of the ramp-down segment and stopping point of a ramp-up segment. The start of a cycling operation is defined by the time instance at which the gross power starts to deviate from the nominal value. The end of the cycling is defined by the time instance at which the gross power is restored to its nominal value.

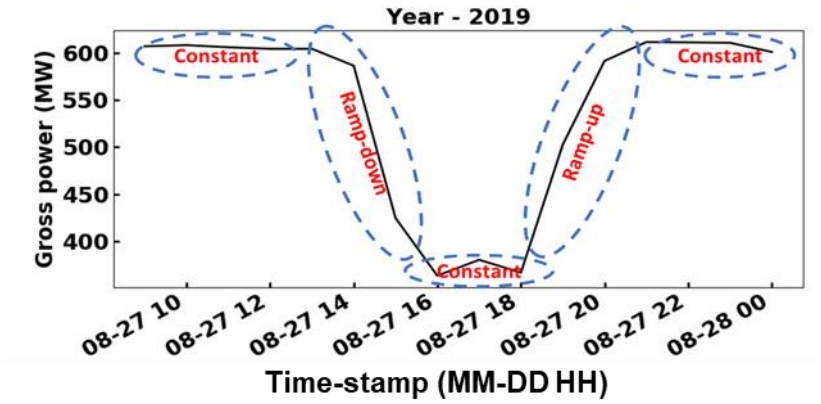

Figure 3.5: Ramp-down, constant and ramp-up operation segments of a cycling operation

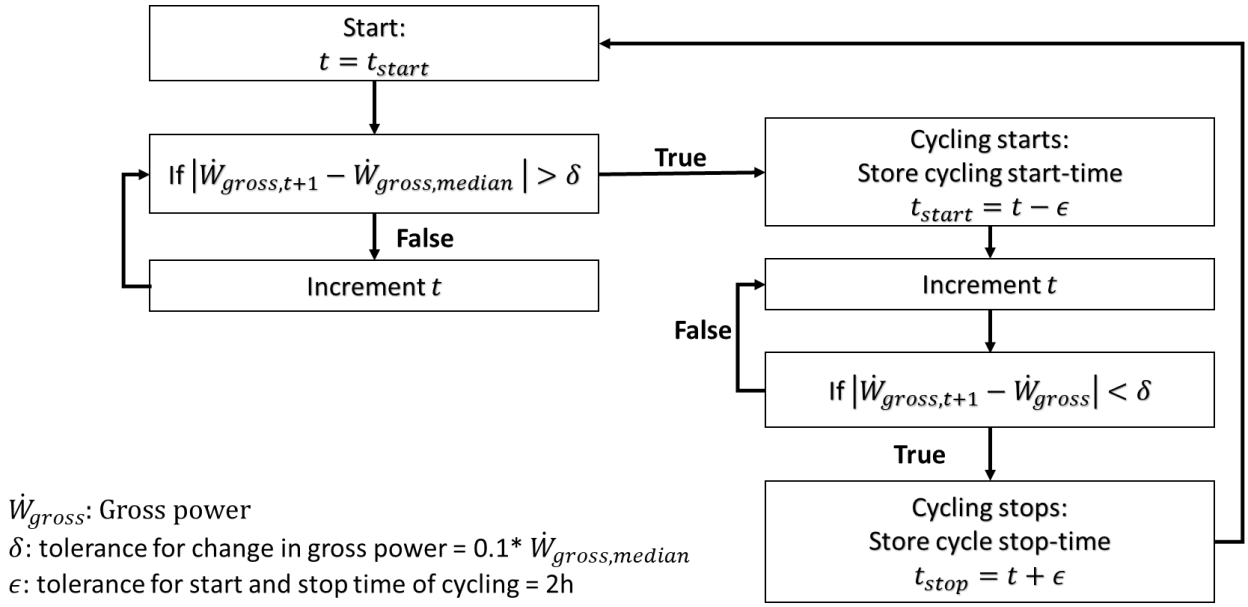

Figure 3.6: Algorithm for identifying cycling from the gross power time-series

Figure 3.6 shows an algorithm for identifying cycling operation from the time-series data of gross power. A program based on this algorithm considers the data points in the time-series sequentially. At $t = 0$, the algorithm checks if the absolute difference between the gross power $(\dot{W}_{gross})$ and median value of the gross power $(\dot{W}_{gross,median})$ is greater than a defined threshold (δ). This threshold defines the magnitude of the fluctuations in the gross power that are considered as cycling. A gross power deviation of approximately 15-20% from the nominal rated gross power

is considered to be a load follow cycling operation [10]. A ramping segment is identified if $\left|\dot{W}_{gross,\,t+1} - \dot{W}_{gross,median}\right| > \delta$. Since the time ($t$) for which this condition becomes true has some delay based on the threshold (δ) and is not the actual starting time of the cycling operation, a tolerance value ϵ is subtracted from it. This time instance is stored as t_{start} of the cycling operation. To find the time instance when the cycling operation ends, the algorithm increments t until $\left|\dot{W}_{gross,\,t+1} - \dot{W}_{gross,median}\right| < \delta$. The time at which this condition is met is further incremented by tolerance of ϵ and stored as the stopping time of the cycling operation. The starting and stopping times of all the cycling operations are found by repeating this algorithm. The algorithm captures both load-follow and on/off cycling operations. In the present study, the value of δ is chosen to be 10% of the median value of the gross power. The value of ϵ is taken to be 2 hours for a reasonable visualization of the cycling operation. In the present study, the value of δ is chosen to be 10% of the median value of the gross power. The value of ϵ is taken to be 2 hours for better visualization of cycling operation.

A few examples of the cycling operations in 2019 identified by the algorithm discussed above are illustrated in Figure 3.7. The range of gross power during cycling operation at different time instances in the year varies significantly. Figure 3.7 (a) shows a typical short-duration cycling operation lasting for about 6 hours and has a gross power range of less than ~100 MW. The cycling operations in Figure 3.7 (b) and Figure 3.7 (c) have a gross power range of ~300MW and ~400MW respectively. The ramp-up and ramp-down segments of these operations are also steeper than those shown in Figure 3.7 (a). Steeper ramp-rates correspond to greater damage to the components. Figure 3.7 (d) shows an on/off operation and the zero gross power corresponds to the shutdown event.

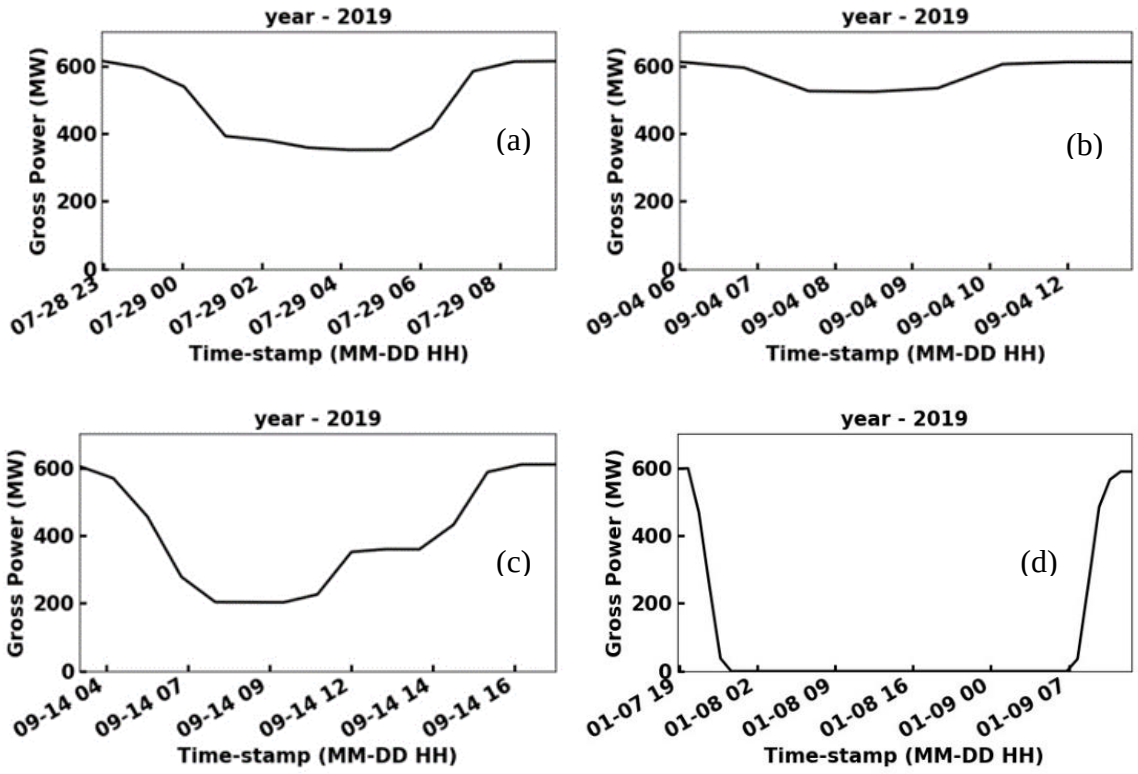

Figure 3.7: Sample cycling operations

In the following analysis, the cycling operations are classified into two categories: load-follow and on/off cycling operations. Load-follow cycling operations are conducted to follow the load demand. There is a large variation in the number of these cycling operations with year. It can be seen from Figure 3.8 that the number of cycling operations was significantly higher during the years 2015-2017. The number of cycling operations is not uniformly distributed across months of the year. In 2019, most of cycling operations were conducted during the months of Aug-Oct.

The gross power range and duration for the load-follow cycling operations vary significantly. Most of the load-follow cycling operations have a duration of 5 to 15 hours and the gross power range is less than 400 MW. A few cycling operations with gross power range greater than 400 MW are shown in Figure 3.10. The gross power falls significantly within a very short duration.

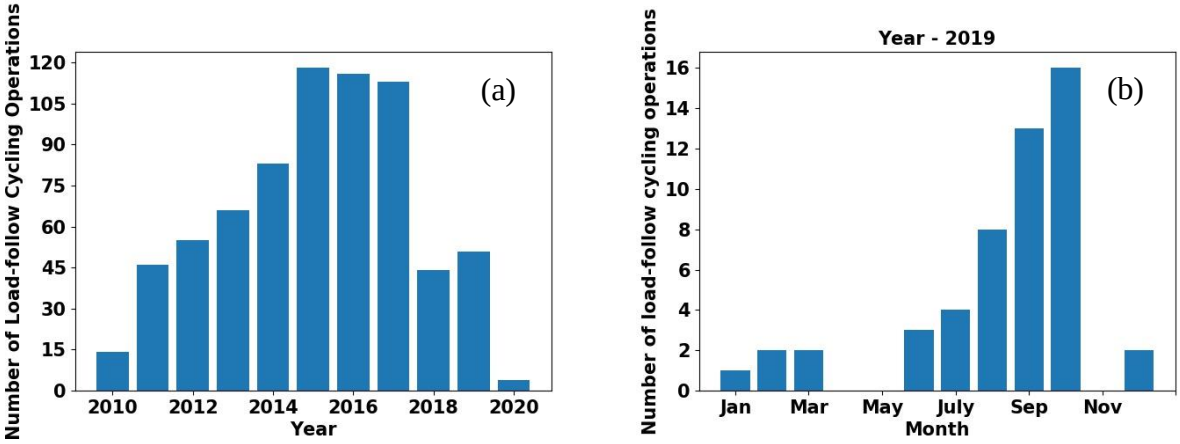

Figure 3.8: Number of load-follow cycling operations vs (a) yeas and (b) month

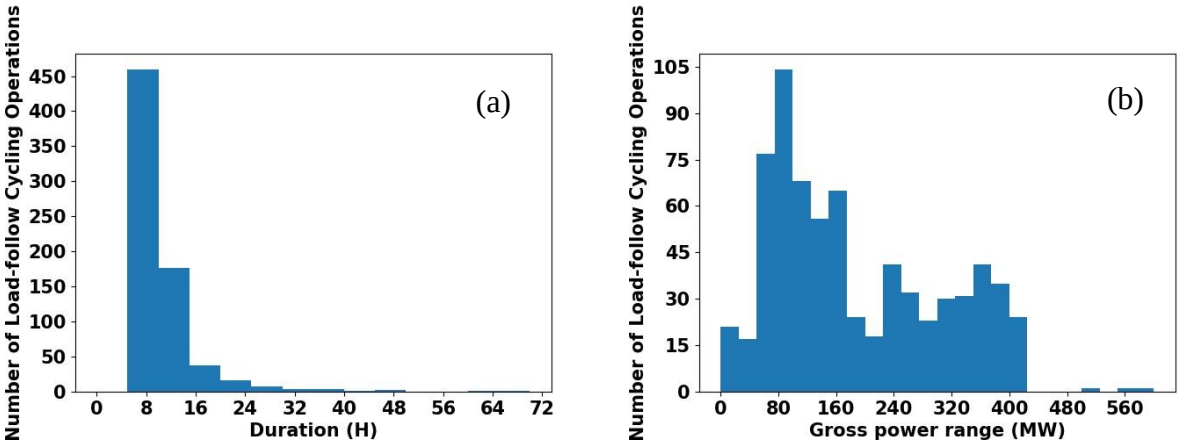

Figure 3.9: Distribution of number of load-follow cycling operations with (a) cycling duration and (b) range of gross-power

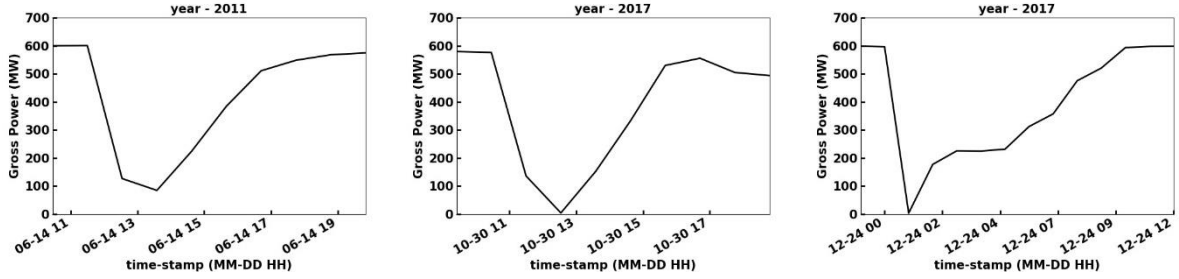

Figure 3.10: Abnormal load-follow cycling operations

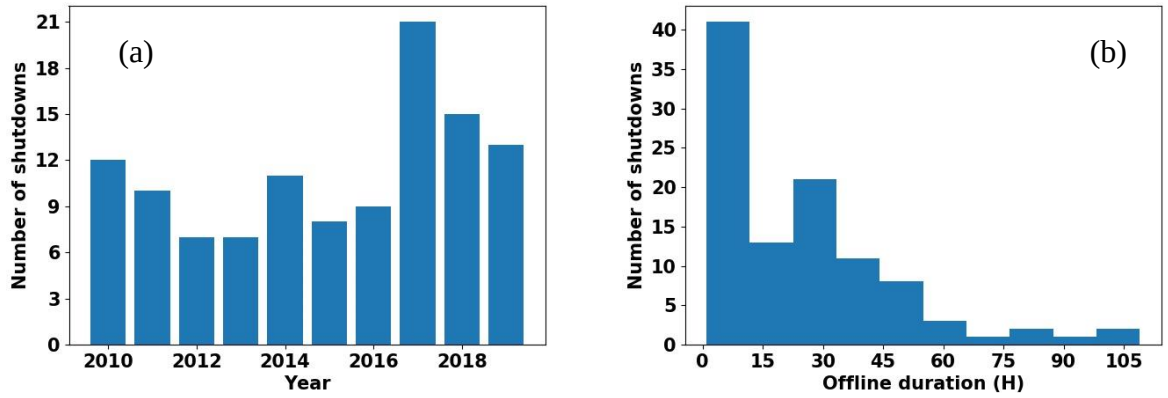

Figure 3.11: (a) Number of shutdowns vs. year (b) Distribution of number of shutdowns with duration (H)

The number of shutdowns (on/off operations) increased in the years 2017 and 2018 as shown in Figure 3.11 (a). The distribution of the number of shutdowns with their duration is shown in Figure 3.11 (b). There were 10 shutdowns with offline hours greater than 5 days which are not included in this figure for better visualization of the distribution. The start-up operations are classified based on the number of offline hours of the shutdown. A warm start refers to startup operation after 12-40 offline hours. If the number of offline hours is lesser than 12, then it's referred to as hot start and cold start corresponds to startup operation after 40 of offline hours. These classifications are based on the [10] for large sub-critical coal-fired power plants. The number of hot, warm and cold startup operations for 2010-2020 is given in Table 3.2.

Table 3.2: Classification of start-up operations for years 2010-2020

Type of start-up operation	Offline hours	Number of start-up operations
Cold	≥ 40	33
Warm	$12\ to\ 40$	64
Hot	≤ 12	41

3.4 Identification of ramp-up, ramp-down and constant operation

The flexibility of power plants for unit commitment and dispatch is characterized by the parameters like start-up time, ramping load gradients, minimum load and minimum up/down time [9]. The operation of the power plant can be divided into ramp-up, ramp-down, and constant

operation segments. The ramp-down and ramp-up segments may consist of smaller segments with different slopes. These smaller segments are clubbed together and classified as a single segment with an average slope. The algorithm for identifying ramp-up, ramp-down and constant segments of operation is described in this section.

The identification of ramp-up, ramp-down, and constant segments begins with the computation of the derivative of gross power.

$$\ddot{W}_{gross,t+1} \approx \frac{\dot{W}_{gross,\,t+1} - \dot{W}_{gross,t}}{\Delta t}$$

The value of $\ddot{W}_{gross,t+1}$ is compared to a threshold value (χ) for classifying each data point as follows,

$$\left|\ddot{W}_{gross,t+1}\right| < \chi \Rightarrow \lambda = 0\ (constant)$$

$$\ddot{W}_{gross,t+1} < -\chi \Rightarrow \lambda = -1\ (ramp - down)$$

$$\ddot{W}_{gross,t+1} > \chi \Rightarrow \lambda = +1\ (ramp - up)$$

λ is the numeric indicator for segment type. A sequence of data points with the same value of λ is considered as one segment. For example, if p data points from time $t = t_k$ to $t = t_{k+p}$ have $\lambda = -1$, then the sequence of these data points is considered as one segment. This segment is characterized by an average slope (m_{avg}), starting gross power $\left(\dot{W}_{gross,\,t_k}\right)$ and the duration of the segment $\left(\Delta t_{seg} = t_{k+p} - t_k\right)$. The average slope for the segment is calculated as follows:

$$m_{avg} = \frac{\dot{W}_{gross,\,t_{k+p}} - \dot{W}_{gross,\,t_k}}{t_{k+p} - t_k}$$

In the present analysis, χ is chosen to be 5% of the median gross power. Figure 3.12 shows the distribution of the number of ramp-up and ramp-down segments with the duration of the segment. The ramp-up operations last for 1-8 hours and ramp-down operation segments last for 1-6 hours. The constant operation segments have a wide range of duration as shown in Figure 3.13. The damage to the steam generator increases with the magnitude of ramp-rate. Figure 3.14 shows the distribution of the number of segments with the ramp rate. A few segments can be seen to have a very large magnitude of ramp-rate.

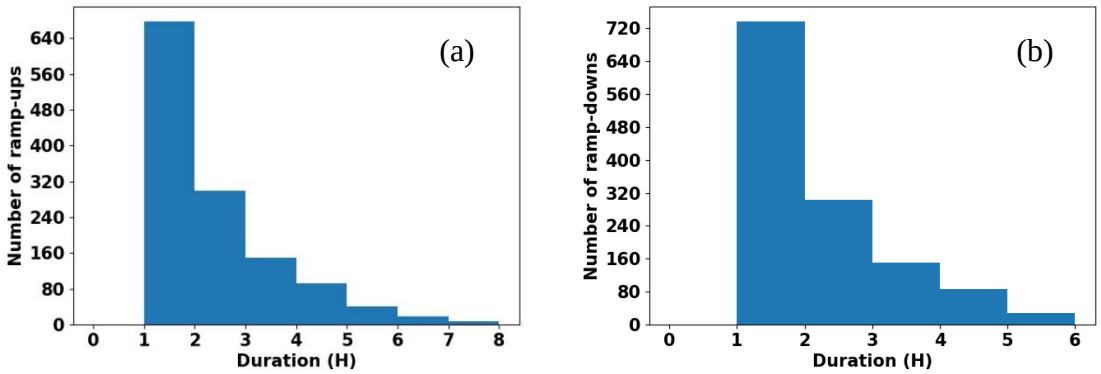

Figure 3.12: Distribution of (a) number of ramp-up operation segments and (b) number of ramp-down operation segments with the duration of the segment

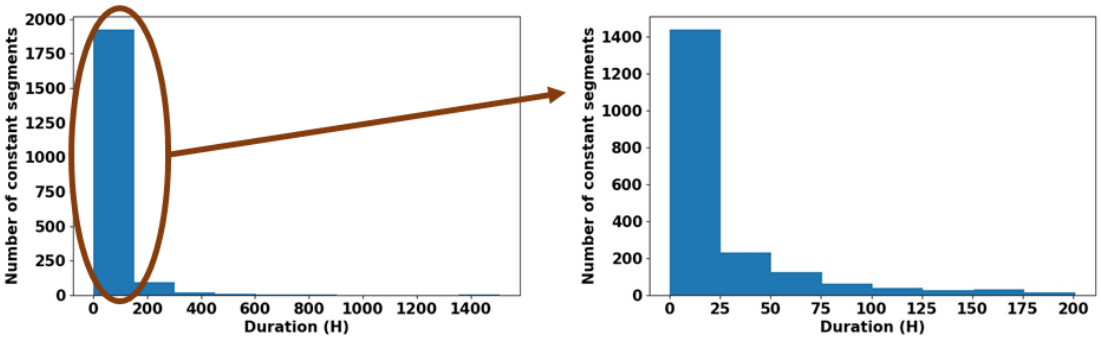

Figure 3.13: Distribution of the number of constant operation segments with the duration of the segment

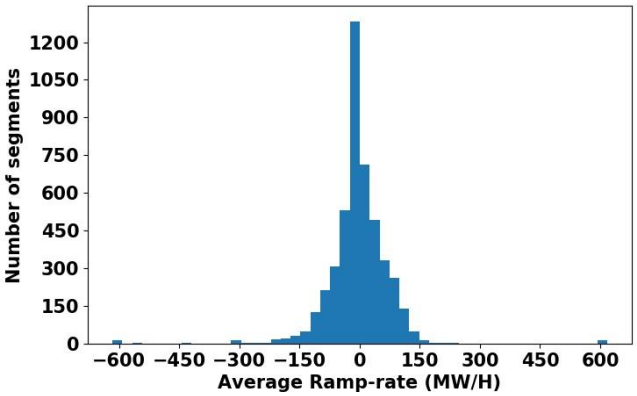

Figure 3.14: Distribution of the number of segments with average ramp-rate (MW/H)

4. ARTIFICIAL NEURAL NETWORK (ANN) FOR ESTIMATING SYSTEM PROPERTIES

4.1 Variation of component properties

Many properties like the steam pressure at the superheater outlet, flue gas temperature at the inlet of air heater, steam pressure at reheater outlet vary during cycling operation. The changes in these properties depend on the changes in the demand for gross power and larger changes cause greater damage to the components. The damage is higher for high-temperature and high-pressure components like superheater, reheater, and air heater. The steam pressure at the superheater outlet, reheater inlet temperature and the flue gas temperature at the air heater inlet are selected as representative properties to monitor in the present study. These properties are known to impact the components' life and vary significantly with gross power.

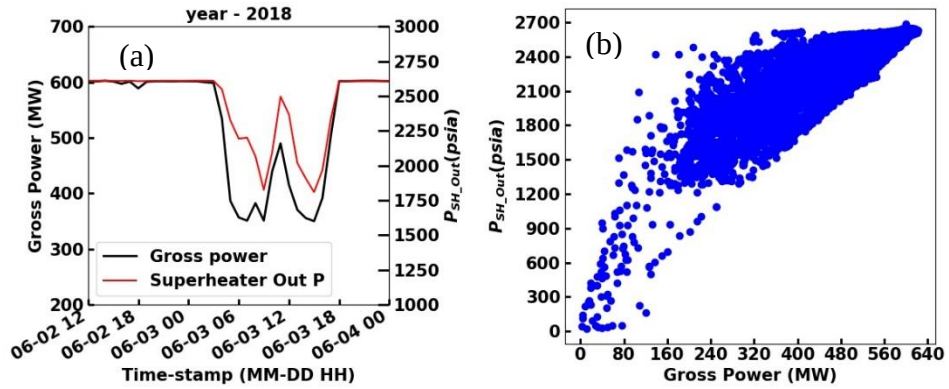

Figure 4.1: (a) Variation of gross power and main steam pressure for a sample cycling operation (b) Variation of main steam pressure with gross power for the years 2010-2019

Figure 4.1 (a) shows the variation of the steam pressure at the superheater outlet (P_{SH_Out}) for a sample cycling operation. The steam pressure has negligible variation when the steam generator is operating at a constant output. As gross power decreases, the value of P_{SH_Out} also decreases and vice versa. However, the relationship between P_{SH_Out} and the gross power is non-linear as shown in Figure 4.1 (b). The performance of the power plant components changes with their age which may lead to different values of P_{SH_Out} for the same gross power. Variation in properties of other components and external conditions also contribute to the variation of P_{SH_Out} for identical gross power.

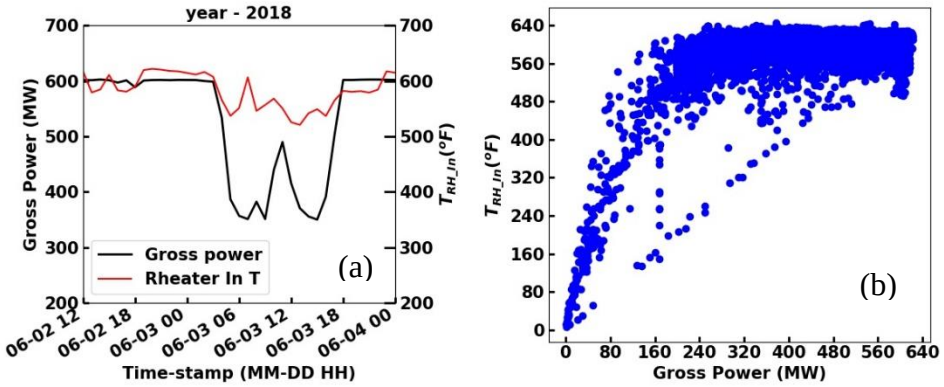

Figure 4.2: (a) Variation of gross power and reheater inlet temperature for a sample cycling operation (b) Variation of reheater inlet temperature with gross power for the years 2010-2019

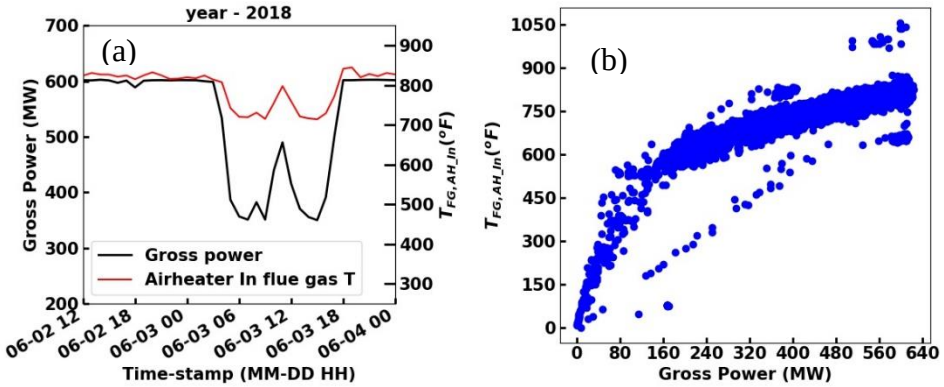

Figure 4.3: (a) Variation of gross power and flue gas temperature at air heater inlet for a sample cycling operation (b) Variation of flue gas temperature at air heater inlet with gross power for the years 2010-2019

The variations of the reheater inlet temperature (T_{RH_In}) and the flue gas temperature at the air heater inlet (T_{FG,AH_In}) are shown in Figure 4.2 and Figure 4.3 respectively. During the cycling operation, the variations of T_{FG,AH_In} and T_{RH_In} also follow the variations of gross power. The changes in these properties are relatively small as compared to the changes in P_{SH_Out}. The T_{RH_In} contains fluctuations which are not directly related to the gross power as can be seen from its variation in the segment with constant gross power. The scatter plots of T_{FG,AH_In} and T_{RH_In} show that the variation of these properties with gross power are relatively small as compared to the variations of $P_{SH_Out}$with gross power. Hence, different ANN models are required to capture the variance in each of these properties. The ANN models developed for the estimation of P_{SH_Out}, T_{FG,AH_In} and T_{RH_In} are described in the following sections. The variation of a few other important system properties is shown in Appendix A.

4.2 Description of the ANN-based model

Artificial Neural Networks (ANN) is a type of machine learning algorithm that is utilized to model non-linear behavior of a system [39]. As illustrated in Figure 4.4, it consists of interconnected nodes arranged in layers. The first layer is called the input layer and the final layer is called the output layer. The layers between the input and the output layers are called the hidden layers. Figure 4.4 shows the ANN model architecture for a gross power profile with a duration of 3 hours. The ANN architecture has 1 input layer, 3 hidden layers, and 1 output layer. The hidden layers have the same number of nodes as the input layer. The inputs to the ANN model include the component properties related to the superheater at the current instance (t_k) and the gross profile of 3 hours duration. The component properties at the current time instance fed to the ANN model are superheater inlet pressure $\left(P_{SH\_In}(t_k)\right)$, superheater outlet pressure $\left(P_{SH\_Out}(t_k)\right)$, superheater outlet temperature $\left(T_{SH\_Out}(t_k)\right)$ and gross power $\left(\dot{W}_{gross}(t_k)\right)$. The gross power profile with a duration of 3 hours is fed as $\left(\dot{W}_{gross}(t_{k+1})\right)$, $\left(\dot{W}_{gross}(t_{k+2})\right)$ and $\left(\dot{W}_{gross}(t_{k+3})\right)$. The output of the model is the main steam pressure corresponding to the input gross power profile.

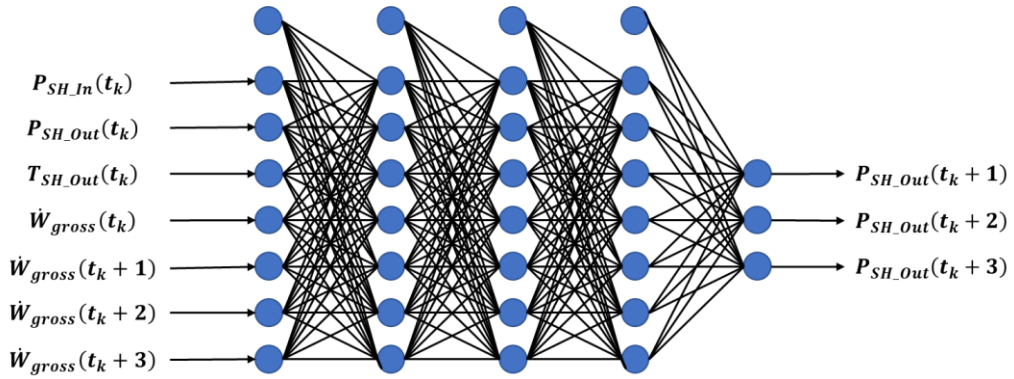

Figure 4.4: ANN architecture for gross power profile duration of 3 hours

The activation of the i^{th} neuron in the l^{th} layer is calculated from the neurons in the previous layer as follows:

$$a_i^{(l)} = g\left(\sum_{j=1}^{s_{l-1}} w_{ij} a_j^{(l-1)} + b^{(l-1)}\right) \quad (1)$$

where s_{l-1} is the number of neurons in the $(l-1)^{th}$ layer, w_{ij} are the weights multiplied to the activations of the previous layer, $b^{(l-1)}$ is the value of the bias neuron and $g()$ is an activation

function such as sigmoid, tanh, rectified linear unit (ReLU), etc which adds non-linearity to the model. The activation function can be different for different layers. The values of the weights and bias are optimized by minimizing a loss function based on the output of the ANN and the true values of the output. For a general neural network with n input variables, K output variables, L layers, s_l nodes in the l^{th} layer, m training examples and weights $\mathbf{w}$, the cost function $J(\Theta)$ with Mean Square Error (MSE) is given as:

$$J(\boldsymbol{w}) = \frac{1}{Km}\sum_{i=1}^{m}\sum_{k=1}^{K}\left(\hat{y}_{k,i} - y_{k,i}\right)^2 \tag{2}$$

The ANN model is developed in two stages. In the first stage the optimal output size is determined by conducting a sensitivity analysis with the length of the gross power profile. The output size of the ANN model is the same as the length of the gross power profile for which the component properties are estimated. After fixing the output size, the ANN model is further refined by considering 15 representative architectures. The ANN architecture with the least error on the validation set is chosen.

4.2.1 Selection of optimal ANN output size

The ANN model aims to estimate the component properties corresponding to a gross power profile. The duration of this gross power profile affects the ANN model's performance. Hence, it is important to identify the duration for which the error is within acceptable limits. The optimal duration for the gross power profile was determined by training ANN models for estimating the main steam pressure at the superheater outlet, for different time lengths of the gross power profile. The data from Coal Creek Station were available as 1-hour averaged time-series for component properties and performance parameters from 2010 to 2019. The dataset for training the ANN model is created by taking each datapoint in the time-series as a current time instance. The following 3 data points in the gross power time series are used as the gross power profile to be fed as input. The 3 data points in the time-series of P_{SH_out} after the current time instance are used as output for training the ANN model. The dataset is normalized to get a range of 0 to 1 for all the input and output variables. The normalized dataset is divided sequentially into three parts: the first 80% of the dataset from 2010 is used for training, the next 10% for validation, and the last 10% for testing.

The steps of the data preprocessing described above for the gross power profile duration of 3 hours are repeated to get datasets corresponding to gross power profile durations of 1 – 20 hours. One ANN architecture is created for each of the gross power profile durations. Each of these ANN architectures has 1 input layer, 3 hidden layers, 1 output layer, and all the hidden layers have the same number of nodes as the input layer.

Each of these 20 models was implemented in Python 3.6 using TensorFlow 2.0 [40]. The training was performed for 100 epochs with a batch size of 256. Rectified Linear Unit (ReLU) activation is applied to the input layer and all the hidden layers. The trainable parameters are optimized by minimizing the Mean Square Error (MSE) between the ANN output and the true value of the main steam pressure corresponding to the input gross power profile. Adam optimizer [41] was used with a constant learning rate of 10^{-4}.

4.2.2 Hyperparameter Tuning

The ANN model is further optimized by tuning additional hyperparameters of ANN architecture such as the number of units in the hidden layers, activation function, and regularization parameters. Fifteen ANN architectures were considered with 14 nodes in the input layer and 10 nodes in the output layer. ANN architectures with different number of hidden layers and different number of neurons in the hidden layers were considered. The number of trainable parameters in the 15 ANN architectures considered is given in Table 4.1. The number of trainable parameters in an ANN architecture represents its complexity. An ANN architecture with high complexity can have high accuracy on the training data set but perform poorly on the validation set. This problem of overfitting is addressed by adding regularization. Regularization was included in some ANN architectures in the form of dropout layers and regularization parameter. ReLU and sigmoid activation functions were considered. The architecture with the lowest validation MSE was chosen.

4.3 Results and Discussion

The ANN models are demonstrated for superheater outlet pressure, reheater inlet temperature, and the flue gas temperature at the air heater inlet for the given cycling gross power profile. A sensitivity study is presented for the superheater outlet pressure with the gross power to assess the predictive capability over the time duration. The MSE for the 20 models, for estimation

of P_{SH_Out}, corresponding to the gross power duration of 1-20 hours is shown in Figure 4.5. The training and validation MSE is lowest for the shortest duration of the gross power profile. The error increases rapidly with the gross power duration up to 6 hours. The curve of validation MSE flattens as the duration of the gross power profile was increased above 15 hours. There is a tradeoff between accuracy and the length of the gross power profile for which the component properties are to be estimated. In this study, the maximum duration for which the MSE is less than 1E-3 was chosen, which was 10 hours.

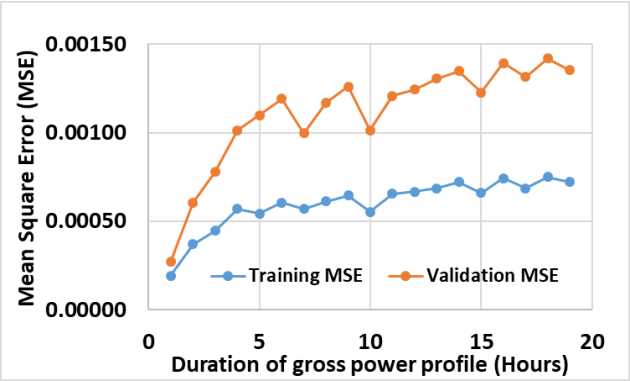

Figure 4.5: Mean square error for P_{SH_Out} vs. gross power profile duration

The hyperparameters of the P_{SH_Out} ANN model with the chosen output duration were tuned by considering fifteen architectures as described in section 4.2.2. The MSE for these ANN architectures is given in Table 4.1. Architectures 9 and 13 have the lowest validation error. Architecture 9 is chosen since it has a lesser number of parameters which leads to a faster computation. The same 15 ANN architectures were also considered for estimation of the T_{RH_In} and T_{FG,AH_In}. It was found that ANN architecture 9 was best suited for these properties as well. The inputs and outputs of the final ANN models for P_{SH_Out}, T_{RH_In} and T_{FG,AH_In} are listed in Table 4.2. Along with the gross power profile, the inputs for the T_{RH_In} ANN model are economizer outlet flue gas temperature $\left(T_{FG,\,Econ\_out}(t_k)\right)$, feedwater temperature $\left(T_{FW}(t_k)\right)$, air heater inlet flue gas temperature $\left(T_{FG,\,AH\_In}(t_k)\right)$ and the gross power at the current time instance. The T_{RH_In} ANN model takes reheater inlet temperature $\left(T_{RH\_In}(t_k)\right)$, reheater outlet temperature $\left(T_{RH\_Out}(t_k)\right)$, economizer outlet flue gas temperature $\left(T_{FG,Econ\_Out}(t_k)\right)$ and the gross power at the current time instance as inputs along with the gross power profile.

Table 4.1: Training and validation Mean Square Error (MSE) for ANN architectures for P_{SH_out}

Sr. No.	No. of trainable parameters	Training MSE	Validation MSE
0	507	0.00093	0.00173
1	360	0.00080	0.00129
2	570	0.00072	0.00124
3	780	0.00072	0.00129
4	990	0.00066	0.00126
5	360	0.00086	0.00146
6	570	0.00102	0.00179
7	780	0.00135	0.00238
8	990	0.00245	0.00433
9	3132	0.00044	0.00085
10	10140	0.00179	0.00308
11	36444	0.00101	0.00191
12	138204	0.00060	0.00125
13	538332	0.00040	0.00085
14	3420	0.00077	0.00141

One of the concerns with ANN models is overfitting. Overfitting occurs when the model performs well on the input data that the model has been trained for but the accuracy is not good for new input data. Overfitting can be checked by plotting the model cost function (MSE) vs epochs. For all the three properties, the training and validation MSE is decreasing with the number of epochs as shown in Figure 4.6. This indicates that the present models do not have the overfitting problem.

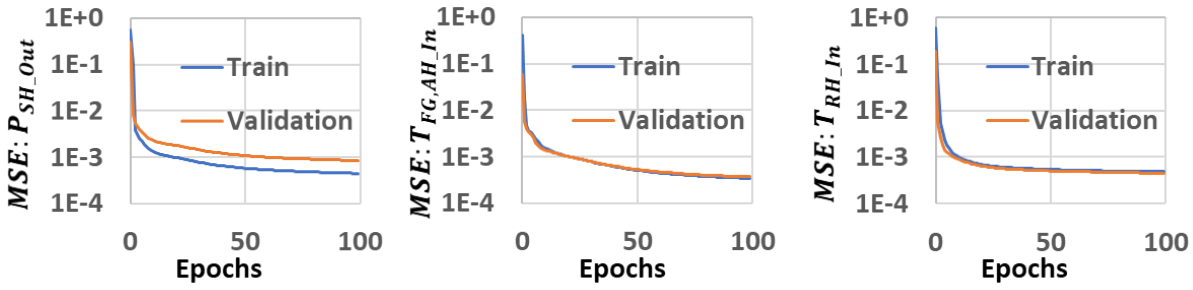

Figure 4.6: MSE vs epoch for superheater outlet pressure, air heater inlet flue gas temperature, and reheater inlet temperature

The MSE of final ANN models for P_{SH_Out}, T_{RH_In} and T_{FG,AH_In} on the training, validation, and test set after 100 epochs are given in Table 4.3. The MSE on the test set for P_{SH_Out} is lower than the validation MSE. This was due to a relatively larger number of cycling operations in the

validation set for P_{SH_Out}. Figure 4.7 shows the true values and predicted value of P_{SH_Out} during a cycling operation from the test set. The green circles represent the history of P_{SH_Out} before cycling operation. The duration of this cycling operation is less than 10 hours and the ANN model was able to estimate the variation of P_{SH_Out}. The MSE for T_{FG,AH_In} on the test set is close to the validation and training set MSE. It can be observed from the Figure 4.7, Figure 4.8 and Figure 4.9 that the maximum error of the P_{SH_Out}, T_{FG,AH_In} and T_{RH_In} on the sample cycling operation at any time instance in the gross power profile is less than 5%.

Table 4.2: Inputs and Outputs for ANN models

Component Property	**ANN model inputs**	**ANN model outputs**
Steam Pressure at Superheater Outlet (P_{SH_Out})	$P_{SH\_In}(t_k)$	$P_{SH\_Out}(t_{k+1})$, $P_{SH\_Out}(t_{k+2})$, … $P_{SH\_Out}(t_{k+10})$
	$P_{SH\_Out}(t_k)$	
	$T_{SH\_Out}(t_k)$	
	$\dot{W}_{gross}(t_k)$	
	$\dot{W}_{gross}(t_{k+1}), \dot{W}_{gross}(t_{k+2})$ … $\dot{W}_{gross}(t_{k+10})$	
Flue gas Temperature at Air heater Inlet ($T_{FG,\,AH\_In}$)	$T_{FG,\,Econ\_out}(t_k)$	$T_{FG,\,AH\_In}(t_k)$, $T_{FG,\,AH\_In}(t_{k+1})$, … $T_{FG,\,AH\_In}(t_{k+10})$
	$T_{FW}(t_k)$	
	$T_{FG,\,AH\_In}(t_k)$	
	$\dot{W}_{gross}(t_k)$	
	$\dot{W}_{gross}(t_{k+1}), \dot{W}_{gross}(t_{k+2})$ … $\dot{W}_{gross}(t_{k+10})$	
Steam Temperature at Reheater Inlet (T_{RH_In})	$T_{RH\_In}(t_k)$	$T_{RH\_In}(t_k)$, $T_{RH\_In}(t_{k+1})$, … $T_{RH\_In}(t_{k+10})$
	$T_{RH\_Out}(t_k)$	
	$T_{FG,\,Econ\_Out}(t_k)$	
	$\dot{W}_{gross}(t_k)$	
	$\dot{W}_{gross}(t_{k+1}), \dot{W}_{gross}(t_{k+2})$ … $\dot{W}_{gross}(t_{k+10})$	

Table 4.3: Training, Validation and Test MSE

	Training MSE	**Validation MSE**	**Test MSE**
P_{SH_out}	0.000449	0.000838	0.000449
T_{FG,AH_In}	0.000343	0.000367	0.000414
T_{RH_In}	0.000485	0.000446	0.001617

The MSE on the test set for T_{RH_In} ANN model is an order of magnitude higher than the validation and training MSE. In section 4.1 it was noted that T_{RH_In} contains fluctuations arising from sources other than gross power. Machine learning algorithms work well when the training, validation and testing data set are derived from the same distribution. The large difference between

the test set MSE and the validation and training set MSE shows that the distribution of data is different between these sets. Further analysis of the power plant data is required to determine the cause of this change and is planned in future work. Additional variables will be included to account for this change in the data distribution of the test set.

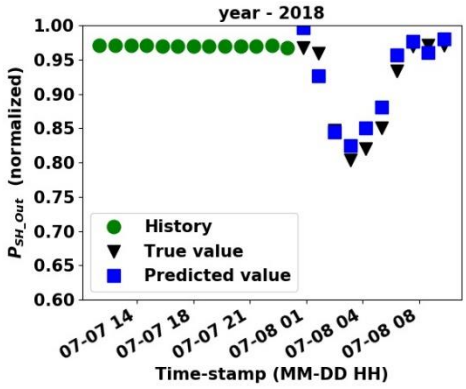

Figure 4.7: True and predicted values of the superheater outlet pressure during cycling

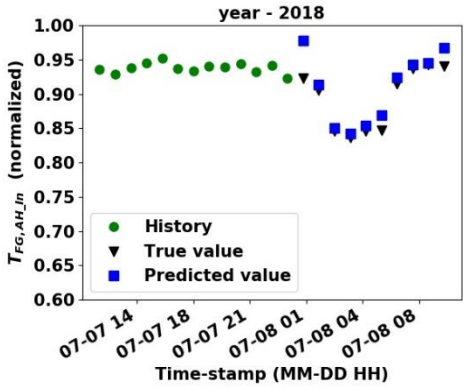

Figure 4.8: True and predicted values of the air heater inlet flue gas temperature during cycling

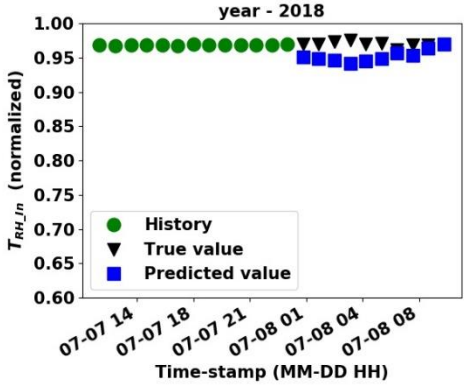

Figure 4.9: True values and predicted values of the reheater inlet temperature during cycling

5. CONCLUSION AND FUTURE WORK

A data-driven modeling approach based on artificial neural networks (ANN) is proposed for establishing a relationship between power plant load cycling and variation of component properties of the steam generator. Data from a coal-fired power plant over 10 years were used in this study. Cycling operations were identified using the gross power time-series data. The data visualization revealed that the component properties such as superheater outlet pressure, reheater inlet temperature, and air heater inlet flue gas temperature are correlated with gross power during cycling operation. However, these properties exhibited a large variation for the same gross power for 10 years. ANN models were developed for the estimation of these properties corresponding to a given gross power profile and initial conditions. A sensitivity study of the model with the gross power profile duration showed that the model accuracy decreased with an increase in the time range of the property predictions. The model was found to perform well for 10 hours. The performance of the models was tested on a sample cycling operation from the test set and the maximum absolute error for all three properties considered in this study was found to be less than 5% during this cycling operation. The MSE on the test set for reheater inlet temperature was an order of magnitude larger than the validation and training set MSE. This indicated that there was a difference in the distribution of data in the test set as compared to the training and validation sets.

The approach described in this study can be extended to build machine learning models for the cost of cycling. Following are the suggestions for future work on this topic:

- As a next step in this study, correlating the property transients with the component damage is recommended to estimate the C&M cost of a cycling operation
- ANN models can be used for estimation of boiler efficiency during cycling operation to estimate the cost due to decreased efficiency
- The sequence of cycling operation events can be related to the sequence of shutdown events using machine learning for estimating the forced outage cost of a cycling operation

APPENDIX A: STEAM GENERATOR SYSTEM PROPERTY VARIATION

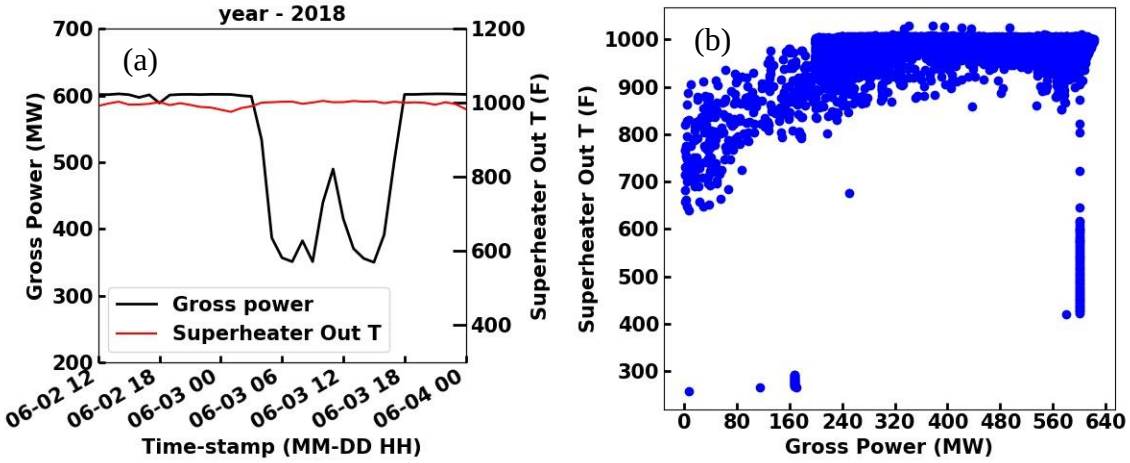

Figure A.1: (a) Variation of gross power and superheater outlet temperature for a sample cycling operation (b) Variation of superheater outlet temperature with gross power for the years 2010-2019

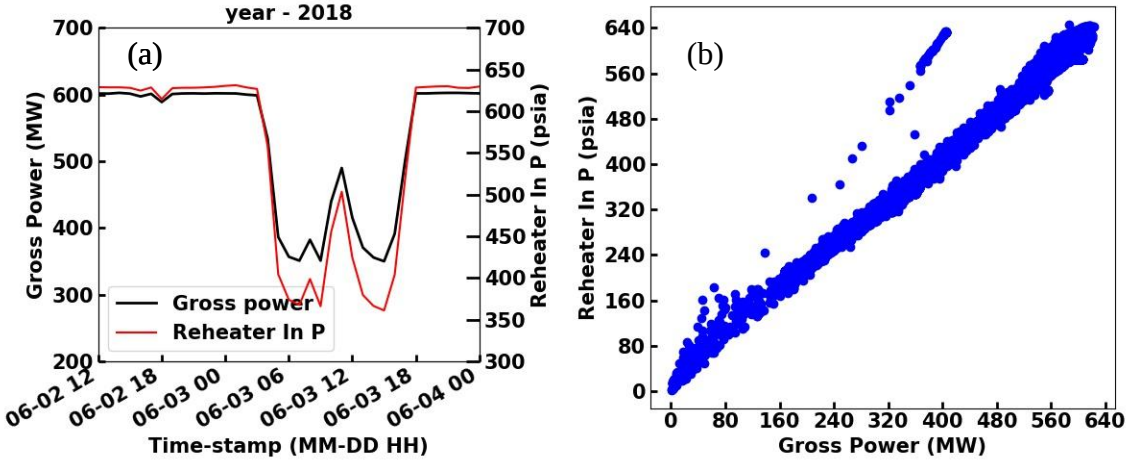

Figure A.2: (a) Variation of gross power and reheater inlet pressure for a sample cycling operation (b) Variation of reheater inlet pressure with gross power for the years 2010-2019

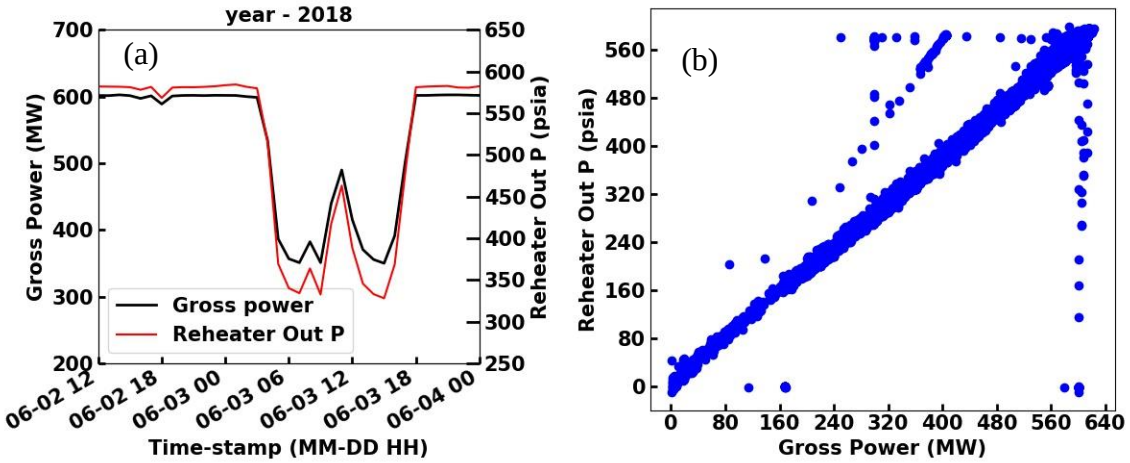

Figure A.3: (a) Variation of gross power and reheater outlet pressure for a sample cycling operation (b) Variation of reheater outlet pressure with gross power for the years 2010-2019

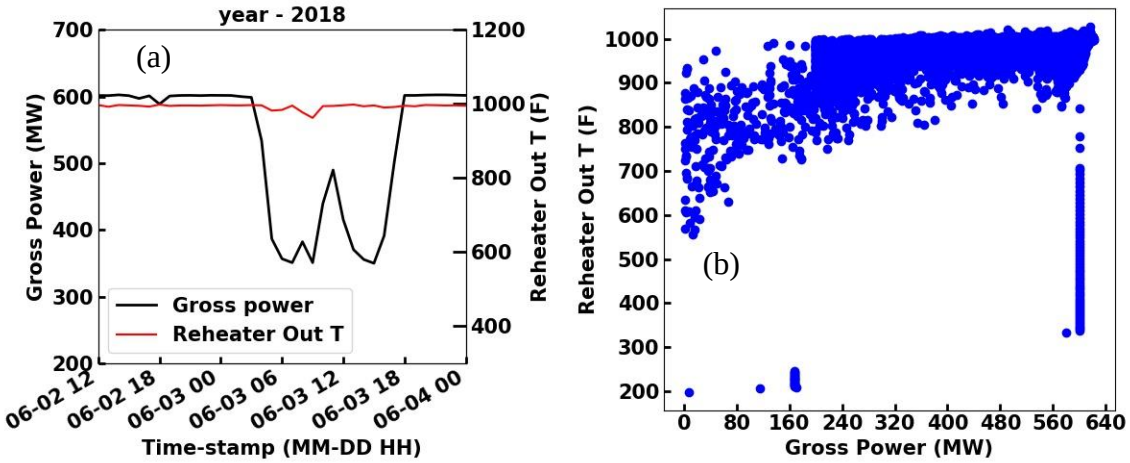

Figure A.4: (a) Variation of gross power and reheater outlet temperature for a sample cycling operation (b) Variation of reheater outlet temperature with gross power for the years 2010-2019

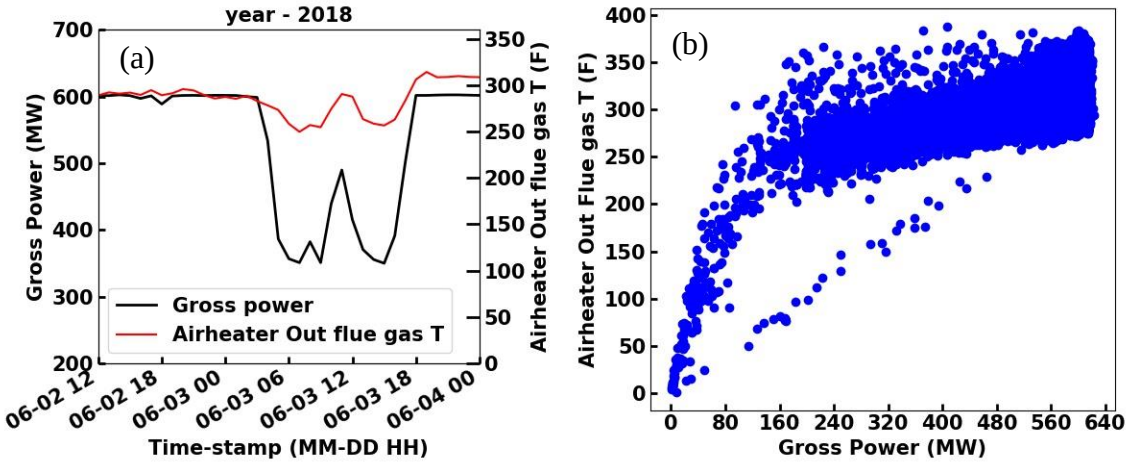

Figure A.5: (a) Variation of gross power and air heater out flue gas temperature for a sample cycling operation (b) Variation of air heater out flue gas temperature with gross power for the years 2010-2019

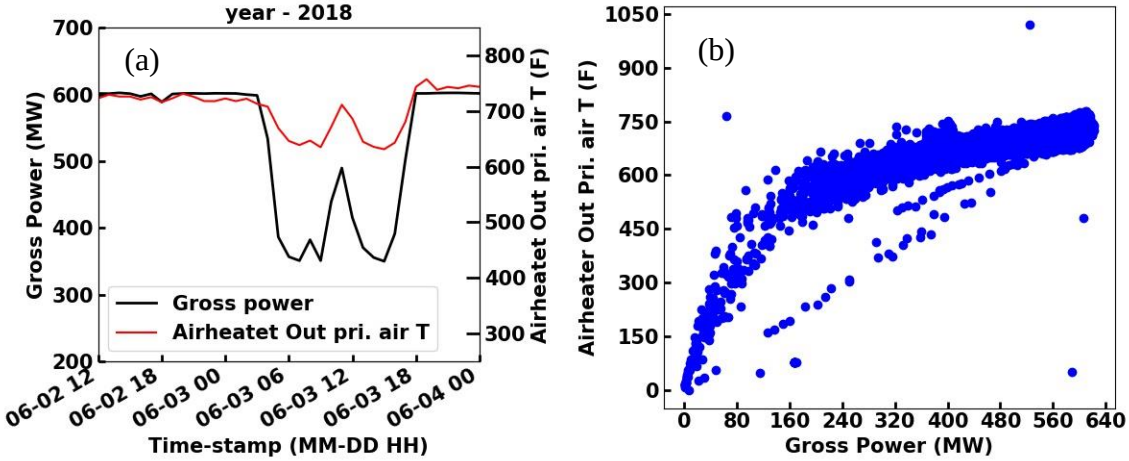

Figure A.6: (a) Variation of gross power and air heater out primary air temperature for a sample cycling operation (b) Variation of air heater out primary air temperature with gross power for the years 2010-2019

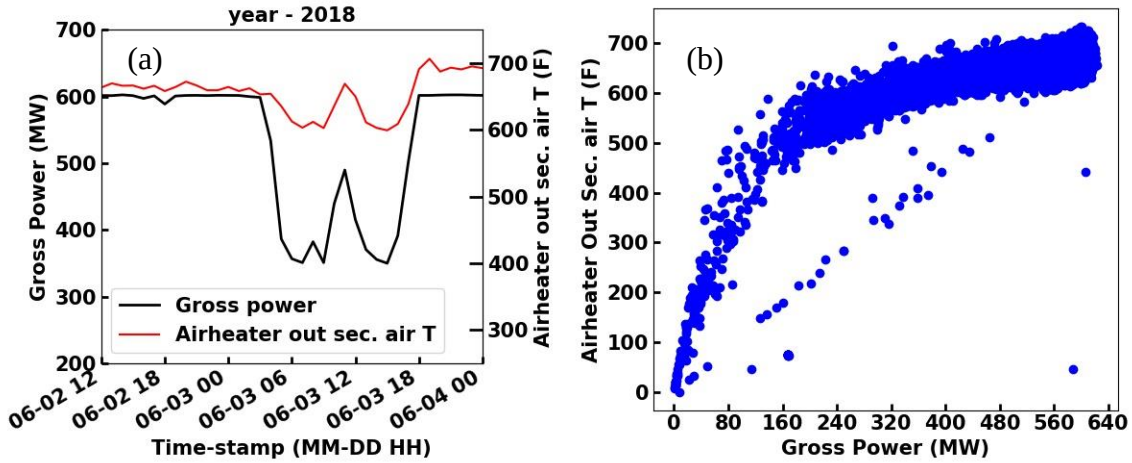

Figure A.7: (a) Variation of gross power and air heater out secondary air temperature for a sample cycling operation (b) Variation of air heater out secondary air temperature with gross power for the years 2010-2019

APPENDIX B: ANN MODEL DETAILS

Table B.1: Number of trainable parameters for different durations of gross power profile

Gross power profile duration	Number of trainable parameters
1	126
2	182
3	248
4	324
5	410
6	506
7	612
8	728
9	854
10	990
11	1136
12	1292
13	1458
14	1634
15	1820
16	2016
17	2222
18	2438
19	2664
20	2900

Table B.2: ANN architectures trained for hyperparameter tuning

Sr. No.	ANN Architecture
0	Input layer No. of nodes = 14 Activation = ReLU → Hidden layer No. of nodes = 7 Activation = ReLU → Hidden layer No. of nodes = 7 Activation = ReLU → Hidden layer No. of nodes = 7 Activation = ReLU → Output layer No. of nodes = 10 Activation = None
1	Input layer No. of nodes = 14 Activation = ReLU → Output layer No. of nodes = 10 Activation = None
2	Input layer No. of nodes = 14 Activation = ReLU → Hidden layer No. of nodes = 14 Activation = ReLU → Output layer No. of nodes = 10 Activation = None
3	Input layer No. of nodes = 14 Activation = ReLU → Hidden layer No. of nodes = 14 Activation = ReLU → Hidden layer No. of nodes = 14 Activation = ReLU → Output layer No. of nodes = 10 Activation = None
4	Input layer No. of nodes = 14 Activation = ReLU → Hidden layer No. of nodes = 14 Activation = ReLU → Hidden layer No. of nodes = 14 Activation = ReLU → Hidden layer No. of nodes = 14 Activation = ReLU → Output layer No. of nodes = 10 Activation = None
5	Input layer No. of nodes = 14 Activation = Sigmoid → Output layer No. of nodes = 10 Activation = None
6	Input layer No. of nodes = 14 Activation = Sigmoid → Hidden layer No. of nodes = 14 Activation = Sigmoid → Output layer No. of nodes = 10 Activation = None
7	Input layer No. of nodes = 14 Activation = Sigmoid → Hidden layer No. of nodes = 14 Activation = Sigmoid → Hidden layer No. of nodes = 14 Activation = Sigmoid → Output layer No. of nodes = 10 Activation = None
8	Input layer No. of nodes = 14 Activation = Sigmoid → Hidden layer No. of nodes = 14 Activation = Sigmoid → Hidden layer No. of nodes = 14 Activation = Sigmoid → Hidden layer No. of nodes = 14 Activation = Sigmoid → Output layer No. of nodes = 10 Activation = None
9	Input layer No. of nodes = 14 Activation = ReLU → Hidden layer No. of nodes = 32 Activation = ReLU → Hidden layer No. of nodes = 32 Activation = ReLU → Hidden layer No. of nodes = 32 Activation = ReLU → Output layer No. of nodes = 10 Activation = None
10	Input layer No. of nodes = 14 Activation = ReLU → Hidden layer No. of nodes = 64 Activation = ReLU → Dropout → Hidden layer No. of nodes = 64 Activation = ReLU → Dropout → Hidden layer No. of nodes = 64 Activation = ReLU → Dropout → Output layer No. of nodes = 10 Activation = None
11	Input layer No. of nodes = 14 Activation = ReLU → Hidden layer No. of nodes = 128 Activation = ReLU → Dropout → Hidden layer No. of nodes = 128 Activation = ReLU → Dropout → Hidden layer No. of nodes = 128 Activation = ReLU → Dropout → Output layer No. of nodes = 10 Activation = None

12	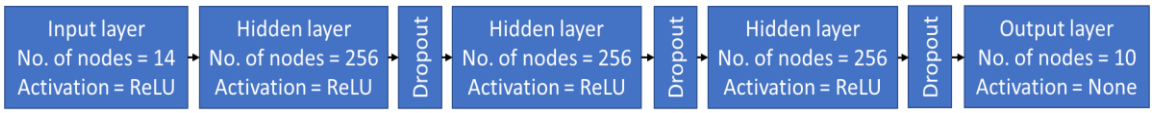
13	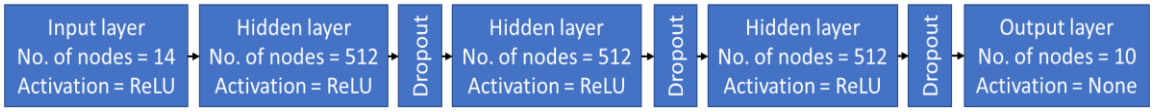
14	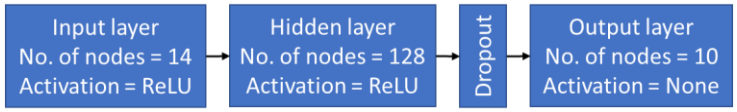

Note: The value of all the dropout layers is 0.5.

REFERENCES

[1] "Electricity in the United States." [Online]. Available: https://www.eia.gov/energyexplained/electricity/electricity-in-the-us.php.

[2] "SHORT-TERM ENERGY OUTLOOK." [Online]. Available: https://www.eia.gov/outlooks/steo/report/electricity.php.

[3] D. Lew, G. Brinkman, N. Kumar, S. Lefton, G. Jordan, and S. Venkataraman, "Finding Flexibility: Cycling the Conventional Fleet," *IEEE Power Energy Mag.*, vol. 11, no. 6, pp. 20–32, 2013, doi: 10.1109/MPE.2013.2277988.

[4] F. Ueckerdt, R. Brecha, and G. Luderer, "Analyzing major challenges of wind and solar variability in power systems," *Renew. Energy*, vol. 81, pp. 1–10, 2015, doi: https://doi.org/10.1016/j.renene.2015.03.002.

[5] P. Eser, A. Singh, N. Chokani, and R. S. Abhari, "Effect of increased renewables generation on operation of thermal power plants," *Appl. Energy*, vol. 164, pp. 723–732, 2016, doi: https://doi.org/10.1016/j.apenergy.2015.12.017.

[6] I. J. Pérez-Arriaga and C. Batlle, "Impacts of Intermittent Renewables on Electricity Generation System Operation," *Econ. Energy Environ. Policy*, vol. 1, no. 2, pp. 3–18, Mar. 2012.

[7] "TODAY IN ENERGY." [Online]. Available: https://www.eia.gov/todayinenergy/detail.php?id=40212.

[8] M. Corio, "Determining the Cost of Cycling and Varied Load Operations: Methodology," Palo Alto, CA, 2002.

[9] A. Schröder, F. Kunz, J. Meiss, R. Mendelevitch, and C. von Hirschhausen, "Current and Prospective Costs of Electricity Generation until 2050," DIW Berlin, German Institute for Economic Research, 2013.

[10] N. Kumar, P. Besuner, S. Lefton, D. Agan, and D. Hilleman, "Power Plant Cycling Costs," United States, 2012.

[11] D. Lew, G. Brinkman, N. Kumar, P. Besuner, D. Agan, and S. Lefton, "Impacts of wind and solar on emissions and wear and tear of fossil-fueled generators," in *2012 IEEE Power and Energy Society General Meeting*, 2012, pp. 1–8, doi: 10.1109/PESGM.2012.6343967.

[12] D. Lew, G. Brinkman, N. Kumar, P. Besuner, D. Agan, and S. Lefton, “Impacts of Wind and Solar on Fossil-Fueled Generators: Preprint,” 2012.

[13] S. A. Lefton, P. M. Besuner, and G. P. Grimsrud, “Managing utility power plant assets to economically optimize power plant cycling costs, life, and reliability,” in *Proceedings of International Conference on Control Applications*, 1995, pp. 195–208, doi: 10.1109/CCA.1995.555681.

[14] A. Shibli, J. Gostling, and F. Starr, “Damage to Power Plants Due to Cycling,” EPRI, Palo Alto, CA, 2001.

[15] E. Eason, A. Merton, and E. Nelson, “Correlating Cycle Duty With Cost at Fossil Fuel Power Plants,” EPRI, Palo Alto, CA, 2001.

[16] K. D. Le *et al.*, “Operational aspects of generation cycling,” *IEEE Trans. Power Syst.*, vol. 5, no. 4, pp. 1194–1203, 1990, doi: 10.1109/59.99370.

[17] K. Van den Bergh and E. Delarue, “Cycling of conventional power plants: Technical limits and actual costs,” *Energy Convers. Manag.*, vol. 97, pp. 70–77, 2015, doi: https://doi.org/10.1016/j.enconman.2015.03.026.

[18] K. Van den Bergh, T. Legon, E. Delarue, and W. D’haeseleer, “Long-term cycling costs in short-term unit commitment models,” in *2016 13th International Conference on the European Energy Market (EEM)*, 2016, pp. 1–5, doi: 10.1109/EEM.2016.7521280.

[19] N. Troy, D. Flynn, M. Milligan, and M. O’Malley, “Unit Commitment With Dynamic Cycling Costs,” *IEEE Trans. Power Syst.*, vol. 27, no. 4, pp. 2196–2205, 2012, doi: 10.1109/TPWRS.2012.2192141.

[20] P. Keatley, “14 - Cost modelling of coal power plant start-up in cyclical operation,” A. B. T.-C. P. P. M. and L. A. Shibli, Ed. Woodhead Publishing, 2014, pp. 358–388.

[21] A. Shibli and J. Ford, “13 - Damage to coal power plants due to cyclic operation,” A. B. T.-C. P. P. M. and L. A. Shibli, Ed. Woodhead Publishing, 2014, pp. 333–357.

[22] S. Holdsworth, “Creep-fatigue interaction in power plant steels,” *Mater. High Temp.*, vol. 28, no. 3, pp. 197–204, Sep. 2011, doi: 10.3184/096034011X13123676561681.

[23] P. Keatley, A. Shibli, and N. J. Hewitt, “Estimating power plant start costs in cyclic operation,” *Appl. Energy*, vol. 111, pp. 550–557, Nov. 2013, doi: 10.1016/J.APENERGY.2013.05.033.

[24] J. Smrekar, M. Assadi, M. Fast, I. Kuštrin, and S. De, “Development of artificial neural network model for a coal-fired boiler using real plant data,” *Energy*, vol. 34, no. 2, pp. 144–152, 2009, doi: https://doi.org/10.1016/j.energy.2008.10.010.

[25] J. Smrekar, D. Pandit, M. Fast, M. Assadi, and S. De, “Prediction of power output of a coal-fired power plant by artificial neural network,” *Neural Comput. Appl.*, vol. 19, no. 5, pp. 725–740, 2010, doi: 10.1007/s00521-009-0331-6.

[26] J. Smrekar, P. Potočnik, and A. Senegačnik, “Multi-step-ahead prediction of NOx emissions for a coal-based boiler,” *Appl. Energy*, vol. 106, pp. 89–99, 2013, doi: https://doi.org/10.1016/j.apenergy.2012.10.056.

[27] X. Liu, X. Tu, G. Hou, and J. Wang, “The dynamic neural network model of a ultra super-critical steam boiler unit,” in *Proceedings of the 2011 American Control Conference*, 2011, pp. 2474–2479, doi: 10.1109/ACC.2011.5991224.

[28] R. Laubscher, “Time-series forecasting of coal-fired power plant reheater metal temperatures using encoder-decoder recurrent neural networks,” *Energy*, vol. 189, p. 116187, 2019, doi: https://doi.org/10.1016/j.energy.2019.116187.

[29] D. Strušnik, M. Golob, and J. Avsec, “Artificial neural networking model for the prediction of high efficiency boiler steam generation and distribution,” *Simul. Model. Pract. Theory*, vol. 57, pp. 58–70, 2015, doi: https://doi.org/10.1016/j.simpat.2015.06.003.

[30] Y. Lv, J. Liu, T. Yang, and D. Zeng, “A novel least squares support vector machine ensemble model for NOx emission prediction of a coal-fired boiler,” *Energy*, vol. 55, pp. 319–329, 2013, doi: https://doi.org/10.1016/j.energy.2013.02.062.

[31] P. Tan *et al.*, “Dynamic modeling of NOX emission in a 660 MW coal-fired boiler with long short-term memory,” *Energy*, vol. 176, pp. 429–436, 2019, doi: https://doi.org/10.1016/j.energy.2019.04.020.

[32] E. Oko, M. Wang, and J. Zhang, “Neural network approach for predicting drum pressure and level in coal-fired subcritical power plant,” *Fuel*, vol. 151, pp. 139–145, 2015, doi: https://doi.org/10.1016/j.fuel.2015.01.091.

[33] G. Irwin, M. Brown, B. Hogg, and E. Swidenbank, “Neural network modelling of a 200 MW boiler system,” *IEE Proc. - Control Theory Appl.*, vol. 142, no. 6, pp. 529–536, 1995, doi: 10.1049/ip-cta:19952293.

[34] H. Rusinowski and W. Stanek, “Neural modelling of steam boilers,” *Energy Convers. Manag.*, vol. 48, no. 11, pp. 2802–2809, 2007, doi: https://doi.org/10.1016/j.enconman.2007.06.040.

[35] H. Rusinowski and W. Stanek, “Hybrid model of steam boiler,” *Energy*, vol. 35, no. 2, pp. 1107–1113, 2010, doi: https://doi.org/10.1016/j.energy.2009.06.004.

[36] S. Lu and B. W. Hogg, “Dynamic nonlinear modelling of power plant by physical principles and neural networks,” *Int. J. Electr. Power Energy Syst.*, vol. 22, no. 1, pp. 67–78, 2000, doi: https://doi.org/10.1016/S0142-0615(99)00036-8.

[37] M. Kljajić, D. Gvozdenac, and S. Vukmirović, “Use of Neural Networks for modeling and predicting boiler’s operating performance,” *Energy*, vol. 45, no. 1, pp. 304–311, 2012, doi: https://doi.org/10.1016/j.energy.2012.02.067.

[38] J. Han, M. Kamber, and J. Pei, “12 - Outlier Detection,” in *The Morgan Kaufmann Series in Data Management Systems*, J. Han, M. Kamber, and J. B. T.-D. M. (Third E. Pei, Eds. Boston: Morgan Kaufmann, 2012, pp. 543–584.

[39] I. Goodfellow, Y. Bengio, and A. Courville, *Deep Learning*. MIT Press, 2016.

[40] M. Abadi *et al.*, “TensorFlow: Large-Scale Machine Learning on Heterogeneous Distributed Systems,” *arXiv e-prints*, p. arXiv:1603.04467, Mar. 2016.

[41] D. P. Kingma and J. Ba, “Adam: A Method for Stochastic Optimization,” *arXiv e-prints*, p. arXiv:1412.6980, Dec. 2014.

VITA

Abhishek Navarkar was born on March 28th, 1993 in Kalyan, India. He graduated from the Indian Institute of Technology (IIT) Gandhinagar in May 2015. He worked as a Scientist at the Defense Research and Development Organization (DRDO), India from 2015-2017. He later pursued his master's degree in mechanical engineering at Purdue University under the guidance of Prof. Jay Gore and Prof. Veeraraghava Raju Hasti graduating in May 2020.